The Plant Cell, Vol. 32: 1218–1239, April 2020, www.plantcell.org © 2020 ASPB.

Interacting Genomic Landscapes of REC8-Cohesin, Chromatin, and Meiotic Recombination in Arabidopsis[CC-BY]

Christophe Lambing,[a] Andrew J. Tock,[a] Stephanie D. Topp,[a] Kyuha Choi,[a,1] Pallas C. Kuo,[a] Xiaohui Zhao,[a] Kim Osman,[b] James D. Higgins,[c] F. Chris H. Franklin,[b] and Ian R. Henderson[a,2]

[a] Department of Plant Sciences, University of Cambridge, Cambridge CB2 3EA, United Kingdom
[b] School of Biosciences, University of Birmingham, Birmingham B15 2TT, United Kingdom
[c] Department of Genetics and Genome Biology, University of Leicester, Leicester LE1 7RH, United Kingdom

ORCID IDs: 0000-0001-5218-4217 (C.L.); 0000-0002-6590-8314 (A.J.T.); 0000-0001-9464-332X (S.D.T.); 0000-0002-4072-3807 (K.C.); 0000-0001-5435-2026 (P.C.K.); 0000-0001-9922-2815 (X.Z.); 0000-0002-0282-4148 (K.O.); 0000-0001-6027-8678 (J.D.H.); 0000-0003-3507-722X (F.C.H.F.); 0000-0001-5066-1489 (I.R.H.)

Meiosis recombines genetic variation and influences eukaryote genome evolution. During meiosis, DNA double-strand breaks (DSBs) enter interhomolog repair to yield crossovers and noncrossovers. DSB repair occurs as replicated sister chromatids are connected to a polymerized axis. Cohesin rings containing the REC8 kleisin subunit bind sister chromatids and anchor chromosomes to the axis. Here, we report the genomic landscape of REC8 using chromatin immunoprecipitation sequencing (ChIP-seq) in Arabidopsis (*Arabidopsis thaliana*). REC8 associates with regions of high nucleosome occupancy in multiple chromatin states, including histone methylation at H3K4 (expressed genes), H3K27 (silent genes), and H3K9 (silent transposons). REC8 enrichment is associated with suppression of meiotic DSBs and crossovers at the chromosome and fine scales. As REC8 enrichment is greatest in transposon-dense heterochromatin, we repeated ChIP-seq in *kyp suvh5 suvh6* H3K9me2 mutants. Surprisingly, REC8 enrichment is maintained in *kyp suvh5 suvh6* heterochromatin and no defects in centromeric cohesion were observed. REC8 occupancy within genes anti-correlates with transcription and is reduced in *COPIA* transposons that reactivate expression in *kyp suvh5 suvh6*. Abnormal axis structures form in *rec8* that recruit DSB-associated protein foci and undergo synapsis, which is followed by chromosome fragmentation. Therefore, REC8 occupancy correlates with multiple chromatin states and is required to organize meiotic chromosome architecture and interhomolog recombination.

INTRODUCTION

The majority of eukaryotes reproduce via meiosis, a specialized cell division that produces four haploid cells from a single diploid parent cell (Villeneuve and Hillers, 2001; Mercier et al., 2015). During meiosis, a single round of DNA replication is followed by two rounds of chromosome segregation that recombines the chromosome complement (Villeneuve and Hillers, 2001; Mercier et al., 2015). In addition, during meiotic prophase I, homologous chromosomes undergo programmed DNA double-strand breaks (DSBs) generated via SPO11 complexes (de Massy, 2013; Lam and Keeney, 2014). Meiotic DSBs are resected to form 3′ single-stranded DNA, which may invade the homologous chromosome, allowing repair as crossovers or noncrossovers (Villeneuve and Hillers, 2001; Mercier et al., 2015). In Arabidopsis (*Arabidopsis thaliana*), ~200 meiotic DSBs are formed, of which ~10 are repaired as crossovers (Mercier et al., 2015). The majority of crossovers in plants exhibit interference, the phenomenon that prevents multiple crossovers from occurring in close proximity along each chromosome pair (Villeneuve and Hillers, 2001; Mercier et al., 2015). The combined effects of meiotic recombination and chromosome segregation strongly influence genetic variation, genome evolution, and adaptation (Kauppi et al., 2004; Barton and Charlesworth, 2009).

Prior to the formation of meiotic DSBs, homologous chromosomes become associated with a polymerized axis structure (Zickler and Kleckner, 1999). In Arabidopsis, this includes the ASY1 HORMA domain protein and the coiled-coil proteins ASY3 and ASY4 (Armstrong et al., 2002; Ferdous et al., 2012; Chambon et al., 2018; Osman et al., 2018; West et al., 2019). During association with the axis, replicated sister chromatids are held together by cohesin complexes containing the meiosis-specific REC8 α-kleisin, which is also required to connect chromatin to the axis (Klein et al., 1999; Cai et al., 2003; Chelysheva et al., 2005; Kim et al., 2010). Meiotic DSBs are proposed to form predominantly within the chromatin loops that become tethered to the axis during interhomolog repair (Zickler and Kleckner, 1999). As meiotic prophase proceeds, the axis is remodeled to form the synaptonemal complex (SC), coincident with the progression of crossover repair (Zickler and Kleckner, 1999; Page and Hawley, 2003). The higher order organization of meiotic chromosomes into a tethered-loop/axis configuration is required for efficient and high-fidelity interhomolog recombination (Zickler and Kleckner, 1999; Page and Hawley, 2003).

[1] Current address: Department of Life Sciences, Pohang University of Science and Technology, Pohang, Gyeongbuk, Republic of Korea.
[2] Address correspondence to irh25@cam.ac.uk.
The author responsible for distribution of materials integral to the findings presented in this article in accordance with the policy described in the Instructions for Authors (www.plantcell.org) is: Ian R. Henderson (irh25@cam.ac.uk).

www.plantcell.org/cgi/doi/10.1105/tpc.19.00866

Epigenetic information on the chromosome loops, including nucleosome positions, histone modifications, histone variants, and DNA methylation, are also known to influence meiotic recombination (Pan et al., 2011; Acquaviva et al., 2013; Choi et al., 2013, 2018; Sommermeyer et al., 2013; Choi and Henderson, 2015; Yelina et al., 2015). For example, DSBs and crossovers typically concentrate in narrow ~1-kb hotspots that are determined to varying degrees by genetic and epigenetic information (Baudat et al., 2013; Lam and Keeney, 2014; Choi and Henderson, 2015). During DSB formation, SPO11 enzymes become covalently bound to target site oligonucleotides (oligos), which can be sequenced to identify sites of recombination initiation (Neale et al., 2005; Pan et al., 2011; Fowler et al., 2014; Lange et al., 2016; Choi et al., 2018). SPO11-oligo sequencing in Arabidopsis and budding yeast (*Saccharomyces cerevisiae*) has revealed meiotic DSB hotspots located in nucleosome-free regions associated with gene regulatory sequences (Pan et al., 2011; Choi et al., 2018). Crossovers in plants also positively associate with H3K4me3 and histone variant H2A.Z, which show 5′ enrichment at transcribed genes (Liu et al., 2009; Choi et al., 2013; Wijnker et al., 2013; He et al., 2017; Kianian et al., 2018). In budding yeast, H3K4me3 tethers DSB hotspots to the Mer2 axis protein via the COMPASS complex Spp1 subunit, showing how chromatin and axis organization can interact to promote meiotic recombination (Acquaviva et al., 2013; Sommermeyer et al., 2013).

Meiotic recombination is also suppressed in broad regions of the chromosomes, including heterochromatin, centromeres, ribosomal gene arrays, sex chromosomes, and mating-type loci (Ellermeier et al., 2010; Vincenten et al., 2015; Yelina et al., 2015; Choi et al., 2018; Underwood et al., 2018). Crossover suppression in these regions may be due to both structural rearrangements and epigenetic marks. Arabidopsis centromeres are organized as megabase arrays of satellite repeats that are surrounded by pericentromeric heterochromatin, which is densely modified with DNA methylation in CG, CHG, and CHH sequence contexts, H3K9me2, H3K27me1, and histone variant H2A.W (Topp and Dawe, 2006; Jacob et al., 2009; Stroud et al., 2013, 2014; Yelagandula et al., 2014). Arabidopsis pericentromeric heterochromatin is suppressed for both meiotic DSBs and crossovers, and loss of H3K9me2 and non-CG DNA methylation increases meiotic recombination in these regions (Choi et al., 2018; Underwood et al., 2018). Crossover hotspots located in Arabidopsis euchromatin have also been directly silenced via RNA-directed DNA methylation and acquisition of H3K9me2 (Yelina et al., 2015). Although the presence of specific heterochromatic marks varies between eukaryotic genomes, suppression of meiotic recombination in centromeric and pericentromeric chromatin is widely observed (Ellermeier et al., 2010; Pan et al., 2011; Fowler et al., 2014; Vincenten et al., 2015; Underwood et al., 2018).

Despite the importance of the tethered-loop/axis architecture and chromatin for meiotic recombination, how they interact to shape DSB and crossover frequency is incompletely understood. REC8-cohesin occupancy has been analyzed via chromatin immunoprecipitation sequencing (ChIP-seq) in budding and fission yeast (*Schizosaccharomyces pombe*) and found to accumulate most strongly in the centromeric regions (Kugou et al., 2009; Ito et al., 2014; Sun et al., 2015; Folco et al., 2017). In fission yeast, REC8 loading in heterochromatin requires H3K9 methylation, further demonstrating the importance of chromatin for meiotic chromosome architecture (Bernard et al., 2001; Nonaka et al., 2002; Mizuguchi et al., 2014; Folco et al., 2017). Within the chromosome arms, transcription exerts an influence on mitotic and meiotic cohesin occupancy, which accumulates at sites of convergent transcription in budding and fission yeast (Lengronne et al., 2004; Mizuguchi et al., 2014; Sun et al., 2015). In this study, we explore REC8 localization in the Arabidopsis genome and its relationship to recombination and chromatin state. The Arabidopsis genome is physically larger than that of budding yeast and fission yeast, with greater gene and transposon numbers and complex megabase-scale centromeres (Tables 1 to 3). Heterochromatic regulation in Arabidopsis also involves additional chromatin modifications, including DNA methylation and H2A.W (Tables 1 to 3; Stroud et al., 2013; Yelagandula et al., 2014). Notably, genome-wide maps of meiotic DSBs, crossovers, and chromatin exist for each of these species, making cross-species comparisons of interest (Tables 1 to 4; Mancera et al., 2008; Pan et al., 2011; Fowler et al., 2014; Choi et al., 2018).

In this work, we map the landscape of Arabidopsis REC8 via ChIP-seq and observe a positive correlation with nucleosome occupancy in multiple euchromatic and heterochromatic chromatin states, including with histone H3K4, H3K9, and H3K27 methylation. At the chromosome scale, REC8 enrichment is greatest in pericentromeric heterochromatin and associates with suppression of meiotic DSBs and crossovers. To test the role of heterochromatin in REC8 enrichment, we repeated ChIP-seq in *kyp suvh5 suvh6* mutants, which lose H3K9me2 and non-CG DNA methylation (Stroud et al., 2014). Surprisingly, REC8 enrichment is maintained in *kyp suvh5 suvh6* heterochromatin and no defects in centromeric cohesion occurred. We observe that patterns of transcription influence REC8 occupancy within genes and transposons. For example, REC8 decreases within *COPIA* transposable elements (TEs) that become transcriptionally upregulated in *kyp suvh5 suvh6*. Together, our work provides a genome-wide map of meiotic cohesin in plants and insights into how chromatin and the axis interact to shape meiotic chromosome architecture and recombination in the Arabidopsis genome.

RESULTS

REC8-Cohesin and Chromatin Organization during Arabidopsis Meiosis

To detect REC8 during meiosis, we inserted 3×HA or 5×Myc epitopes into a *REC8* genomic clone that uses the endogenous promoter and transformed *rec8-3* heterozygotes (Cai et al., 2003; Chelysheva et al., 2005). We assessed complementation of *rec8* by cytological analysis of meiosis in the resulting transformants (Figure 1A). *rec8* shows severe meiotic defects in chromatin compaction, axis formation, and the presence of chromosome fragmentation, which cause complete sterility (Figure 1A; Bhatt et al., 1999; Cai et al., 2003; Chelysheva et al., 2005). We observed that transformation with the hemagglutinin (HA)- and Myc epitope–tagged *REC8* constructs fully complemented axis formation during prophase I, the presence of five bivalents at metaphase I,

Table 1. Genome Architecture in Arabidopsis, Budding Yeast, and Fission Yeast

Species	Genome Size (Mb)	Chromosome No.	Genes	Transposable Elements	DNA TEs	RNA TEs
S. pombe	12.6	3	5,130	187	None	TF2 LTR
S. cerevisiae	12.1	16	6,002	50	None	Ty1-Ty5 LTR
Arabidopsis	119.2	5	27,655	3,901	Ac/Ds, CACTA/En-SPM, Mu, Helitron, Pogo/Tc1/Mariner	Gypsy, Copia, SINE, LINE1

and chiasmata formation in *rec8-3* (Figure 1A; Supplemental Table 1).

To analyze REC8 accumulation on meiotic chromosomes, we immunostained male meiocytes using α-HA or α-Myc antibodies and stained chromatin with 4′,6-diamidino-2-phenylindole (DAPI; Figure 1B; Supplemental Figure 1A). We observed colocalization of REC8 with chromatin from leptotene onward, including within heterochromatin (Figure 1B; Supplemental Figure 1A). REC8 and chromatin colocalized as pairing and synapsis occurred, with strong costaining of the paired axes at pachytene (Figure 1B; Supplemental Figure 1A). The tagged REC8 proteins persisted on bivalents through diakinesis and metaphase I (Figure 1B; Supplemental Figure 1A), as reported previously (Cai et al., 2003; Chelysheva et al., 2005). No signal was detected in the nontransgenic wild-type meiocytes, or somatic cells of *REC8* epitope-tagged lines (Figure 1B; Supplemental Figure 1A). This demonstrates specific detection of REC8-HA and REC8-Myc proteins with the expected localization on meiotic chromosomes (Cai et al., 2003; Chelysheva et al., 2005).

To visualize chromatin organization during meiosis, we immunostained for euchromatic (H3K4me3) and heterochromatic (H3K9me2 and H3K27me1) histone modifications, together with the SC protein ZYP1 (Figure 1C; Higgins et al., 2005). During late prophase I, when ZYP1 polymerization was complete, we observed clear differentiation of euchromatin and heterochromatin, with ZYP1 signal continuous through both chromatin types (Figure 1C). To assess axis and SC signal through the centromeres, we performed fluorescence in situ hybridization for the satellite repeat *CEN180* and coimmunostained for ZYP1 or the SMC3 cohesin subunit (Figure 1D). At the zygotene–pachytene transition, we observed *CEN180*-positive regions, through which the SMC3 and ZYP1 signals were continuous (Figure 1D). Together, these data show that the SC and cohesin form a continuous axis through Arabidopsis euchromatin, heterochromatin, and the centromeres during meiosis.

Profiling the Genomic Landscape of REC8 Enrichment by ChIP-Seq

To generate a genome-wide map of REC8 enrichment, we sought to use the HA- and Myc epitope–tagged lines to perform ChIP-seq. As REC8 is specifically expressed during meiosis (Figure 1B; Supplemental Figure 1A; Cai et al., 2003; Chelysheva et al., 2005), we collected unopened flower buds for ChIP. These flowers contain all stages of meiosis, although prophase I has the longest duration (~31 of ~33 h; Armstrong, 2013), during which REC8 associates with chromosomes (Figure 1B; Supplemental Figure 1A). We performed immunoblotting on meiotic-stage flowers before and after α-HA or α-Myc immunoprecipitation, revealing specific bands of the expected size (77.2-kD REC8-HA and 84.2-kD REC8-Myc) in addition to bands with an apparent ~20-kD higher molecular mass, likely representing phosphorylated forms of REC8 (Figure 2A; Supplemental Figure 1B). For example, slow-migrating forms of REC8 have also been observed in yeast and mice, which are caused by phosphorylation (Watanabe and Nurse, 1999; Kitajima et al., 2003). A nonspecific α-HA band was detected in input samples from *REC8-HA rec8* and the wild type (Columbia [Col]), but this band was greatly depleted after immunopurification (Figure 2A).

Approximately 10 g of unopened flowers collected from pools of plants was used for ChIP from *REC8-HA rec8*, and the resulting DNA was used to construct sequencing libraries (Supplemental Table 2). We analyzed genome coverage values from biological replicate REC8-HA ChIP-seq libraries, which were highly correlated when compared at varying physical scales (e.g., 10-kb windows, Spearman's rank-order correlation coefficient $r_s = 0.92$; Supplemental Table 3). To test the specificity of REC8 enrichment, we repeated α-HA ChIP from untagged Col flowers, and the resulting DNA was used to generate a sequencing library. The Col library yielded 3,681,603 read pairs of which only 0.75% mapped to the Arabidopsis genome, compared with mapping rates of 91.34 to 93.22% of reads from the *REC8-HA* libraries

Table 2. Chromatin in in Arabidopsis, Budding Yeast, and Fission Yeast

Species	Heterochromatin	Euchromatin	Centromere	Polycomb/ H3K27me3
S. pombe	H3K9me3	H3K4me1, H3K4me2, H3K4me3, H3K36me3, H2A.Z, H3/H4-Acetyl	Complex (35, 65, and 110 kb)	No
S. cerevisiae	Sir2-mediated deacetylation	H3K4me1, H3K4me2, H3K4me3, H3K36me3, H2A.Z, H3/H4-Acetyl	Point (120 bp)	No
Arabidopsis	H3K9me2, H3K27me1, DNA CG CHG CHH, H2A.W	H3K4me1, H3K4me2, H3K4me3, H3K36me3, H2A.Z, H3/H4-Acetyl	Complex (~1 to 5 Mb)	Yes

Table 3. Meiotic Recombination in Arabidopsis, Budding Yeast, and Fission Yeast

Species	cM	cM/Mb	ZMM	Interference distance	Pachytene axis μM
S. pombe	2,200	174.2	–	–	–
S. cerevisiae	4,420	366.2	ZIP2, ZIP3, ZIP4, SPO16, MER3, MSH4, MSH5	Megabases	34
Arabidopsis	398	3.3	HEI10, SHOC1, PTD1, MER3, MSH4, MSH5	Megabases	179

Dashes indicate no data.

(Supplemental Table 2). This demonstrates the low background obtained by our ChIP-seq protocol.

To further analyze the specificity of α-HA ChIP enrichment, three regions were analyzed by qPCR from *REC8-HA rec8* versus untagged Col (Figure 2B; Supplemental Table 4). The regions analyzed were heterochromatic *ATHILA* and *ATHILA6B* TEs, and the 5′ end of a euchromatic gene (At2g02480), which were predicted to show high REC8 occupancy (Figure 2B; Supplemental Table 4). For each region, significantly greater enrichment was measured from ChIP relative to input for *REC8-HA rec8* compared with untagged Col, with highest REC8 enrichment within the transposons (Figure 2B; Supplemental Table 4), further confirming the specificity of our protocol. Finally, we analyzed α-Myc ChIP-seq data from *REC8-Myc rec8* plants; they showed a positive correlation with *REC8-HA* data (e.g., 10 kb windows, $r_s = 0.83$ to 0.86; Figure 3A; Supplemental Table 3). This demonstrates that we obtain reproducible signal when performing REC8 ChIP using two independent epitopes. Because of the high correlation of REC8-HA and REC8-Myc data, for subsequent analysis we focused on REC8-HA ChIP-seq data.

To assess REC8 enrichment at the fine scale, we analyzed ChIP-seq values (per-base coverage values normalized by total library coverage) and compared them with chromatin and recombination data (Figure 2C; Table 4). These data included (1) nucleosome occupancy (micrococcal nuclease sequencing [MNase-seq]; Choi et al., 2016); (2) markers of heterochromatin H3K9me2 (ChIP-seq), DNA methylation (bisulfite sequencing), and small interfering RNAs (small interfering RNA [siRNA] sequencing; Lee et al., 2012; Stroud et al., 2013); (3) histone marks enriched at euchromatic genes H3K4me3 (Choi et al., 2018), H3K4me2, H3K4me1 (ChIP-seq), and mRNA from flowers or male meiocytes (RNA sequencing [RNA-seq]; Walker et al., 2018); (4) the Polycomb histone mark H3K27me3 (ChIP-seq; Zhu et al., 2015); and (5) SPO11-1-oligos that mark meiotic DSBs (Choi et al., 2018) and crossovers mapped by sequencing Col × Landsberg *erecta* F_2 plants (Serra et al., 2018; Rowan et al., 2019).

Table 4. Genomic Maps of Chromatin, Transcription, and Meiotic Recombination in Arabidopsis

Data Set	Reference	Tissue[a]
REC8 ChIP-seq	This study	Floral buds
H3K9me2 ChIP-seq	This study	Floral buds
SPO11-1-oligos	Choi et al., 2018	Floral buds
Nucleosome MNase-seq	Choi et al., 2018	Floral buds
H3K4me1 ChIP-seq	This study	Floral buds
H3K4me2 ChIP-seq	This study	Floral buds
H3K4me3 ChIP-seq	Choi et al., 2018	Floral buds
DNA methylation BS-seq	Stroud et al., 2013	Seedlings
siRNA-seq	Lee et al., 2012	Immature inflorescences
Flower mRNA RNA-seq	Choi et al., 2018	Floral buds
Meiocyte mRNA RNA-seq	Walker et al., 2018	Floral buds
H3K27me3 ChIP-seq	Zhu et al., 2015	Floral buds
Crossovers	Rowan et al., 2019	Seedlings

BS-seq, bisulfite sequencing; siRNA-seq, siRNA sequencing.
[a]The tissue collected for data generation is listed.

With reference to a representative 65-kb region of chromosome 3, we observed a positive correlation between REC8 and nucleosome occupancy, both of which negatively correlated with SPO11-1-oligos (Figure 2C). High REC8 enrichment was evident within different types of sequence element and chromatin state; for example, (1) a transcriptionally silent *LINE1* TE (AT3TE37690) that showed high nucleosome density, DNA methylation, H3K9me2, and siRNAs, and suppressed SPO11-1-oligos; (2) expressed genes (e.g., *TMKL1*, *PLL22*, *HCR1*, and *F-box*) that showed high nucleosome occupancy with H3K4me1, H3K4me2, and H3K4me3 modifications; and (3) a H3K27me3-silenced gene (*ABI3*; Figure 2C). Therefore, we next sought to explore REC8 ChIP-seq enrichment at multiple scales and within different sequence contexts in relation to chromatin and recombination data sets.

REC8 Enrichment in Euchromatin and Heterochromatin at the Chromosome Scale

We compared REC8-HA ChIP-seq enrichment with markers of euchromatin and heterochromatin and meiotic recombination along the Arabidopsis chromosomes (Figure 3). For genome-wide analysis, REC8-HA ChIP and input data were used to calculate windowed $\log_2$(ChIP/input) enrichment values. At the chromosome scale, REC8-HA enrichment was greatest in the centromeres and in proximal heterochromatin, which positively correlated with nucleosome occupancy ($r_s = 0.68$; Figure 3A). Because of pericentromeric REC8-HA enrichment, we also observed positive correlations with TE density ($r_s = 0.74$), DNA methylation in CG ($r_s = 0.79$), CHG ($r_s = 0.72$), and CHH ($r_s = 0.72$) sequence contexts, and the heterochromatic histone modifications H3K9me2 ($r_s = 0.78$) and H3K27me1 ($r_s = 0.75$), and histone variant H2A.W ($r_s = 0.83$; Figure 3A; Stroud et al., 2013; Yelagandula et al., 2014). These relationships were further strengthened if the pericentromeres were considered separately from the chromosome arms (Figure 3B). Hence, as in budding and fission yeasts (Kugou et al., 2009; Ito et al., 2014; Sun et al., 2015; Folco et al., 2017), the strongest REC8 ChIP-seq enrichment in Arabidopsis is observed in proximity to the centromeres.

To provide cytological support for the trends observed via ChIP-seq, we analyzed spread nuclei at pachytene stage that were

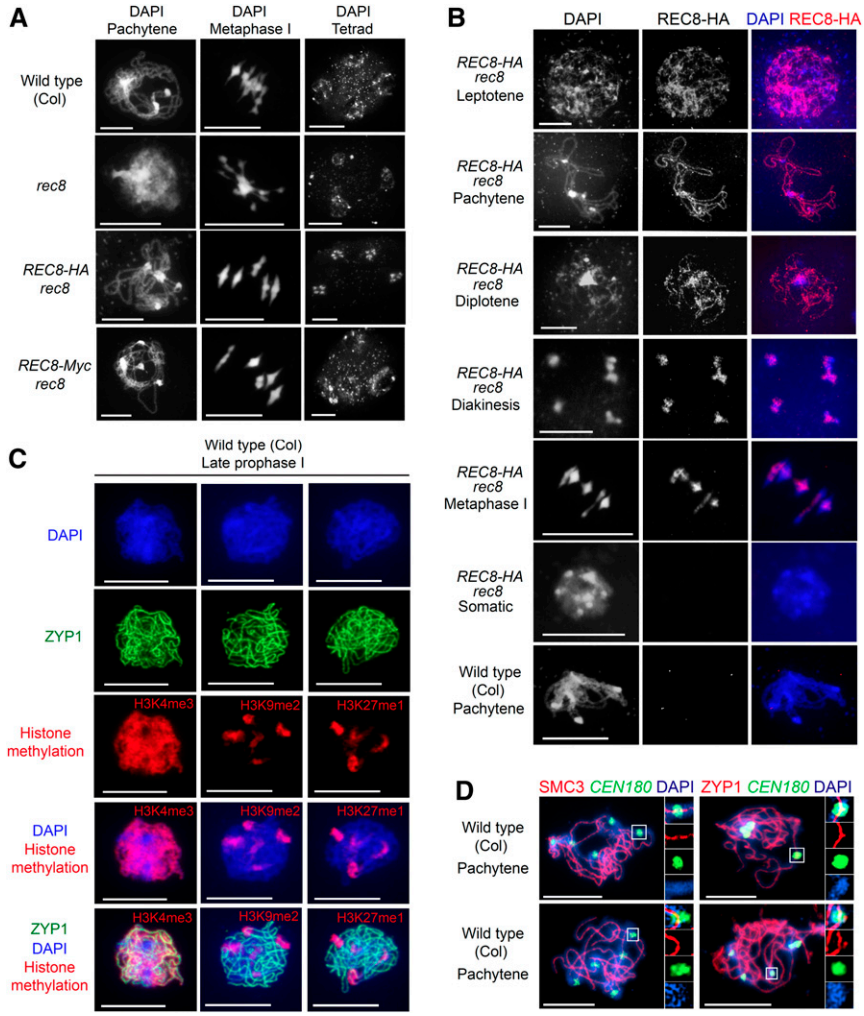

Figure 1. REC8-Cohesin, Chromatin, and the SC during Arabidopsis Meiosis.

(A) DAPI-stained spreads of wild-type (Col), *rec8*, *REC8-HA rec8*, and *REC8-Myc rec8* male meiocytes, at the labeled stages of meiosis.
(B) Male meiocytes from the wild type or *REC8-HA rec8* immunostained for REC8-HA (red) and stained for DNA (DAPI, blue), at the labeled stages.
(C) Male meiocytes immunostained for ZYP1 (green) or histone methylation (red; H3K4me3, H3K9me2, or H3K27me1) and stained for DNA (DAPI, blue) in the wild type (Col), during late prophase I.
(D) Male meiocytes at pachytene stage immunostained for SMC3 (red) or ZYP1 (red) and stained for DNA (DAPI, blue). Fluorescence in situ hybridization was performed against the *CEN180* centromeric satellite sequence (green). Inset images show magnifications of the *CEN180*-positive regions. All scale bars = 10 μm.

immunostained for REC8-HA and chromatin stained with DAPI (Figure 3C). We tracked and quantified axial REC8-HA signal as it transversed heterochromatin (Figure 3C). We centered analysis on heterochromatin over a distance of 100 pixels (equivalent to ~6.4 μM) in 20 sections from a total of 10 meiocytes (Figure 3C). We observed that mean REC8-HA and DAPI signal intensity were significantly correlated over the tracked regions (r_s = 0.94, P = 4.07 × 10^{-47}). These cytological data are consistent with REC8-HA ChIP-seq enrichment correlating with nucleosome-dense heterochromatin (Figures 3A and 3B).

Because of REC8-HA enrichment in pericentromeric heterochromatin, genome-wide negative correlations between REC8-HA and gene density (r_s = −0.70) and the gene-associated chromatin modifications H3K4me1 (r_s = −0.63), H3K4me2 (r_s = −0.74), H3K4me3 (r_s = −0.75), H2A.Z (r_s = −0.62), and H3K27me3 (r_s = −0.26) were observed (Figures 3A and 3B; Yelagandula et al., 2014). When the chromosome arms were considered separately, a weaker positive correlation between REC8-HA and nucleosome occupancy was observed (r_s = 0.40; Figure 3B). The chromosome arms undergo the greatest levels of meiotic DSBs (measured via SPO11-1-oligos) and crossovers (Figure 3B). However, as noted previously (Choi et al., 2018; Underwood et al., 2018), while crossovers and SPO11-1-oligos are positively correlated (genome-wide r_s = 0.63, chromosome arms r_s = 0.46, pericentromeric r_s = 0.85), they show considerable variation in their relative frequencies within the chromosome arms

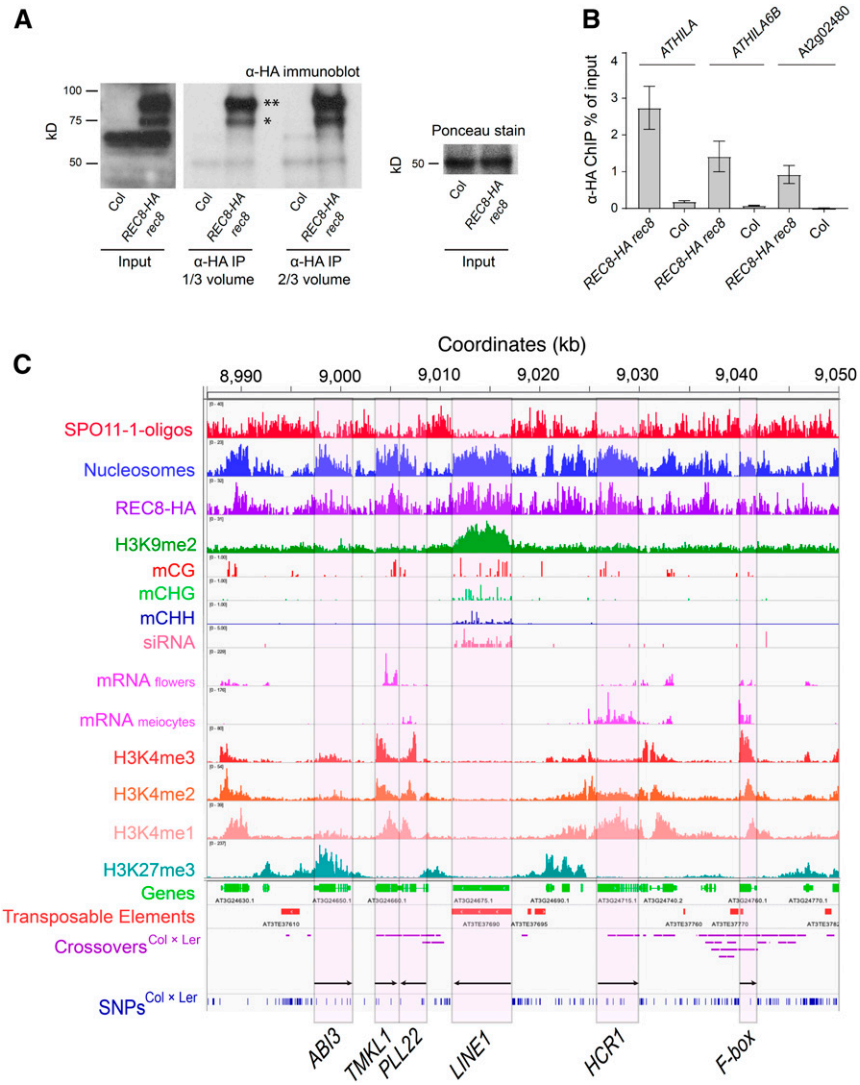

Figure 2. Profiling the Genomic Landscape of Arabidopsis REC8 by ChIP-Seq.

(A) Immunoblot of the wild-type (Col) and *REC8-HA rec8* floral extracts before (input) and after α-HA immunoprecipitation (IP). Ponceau staining of the input lane is shown. The predicted molecular mass of REC8-HA is 77.2 kD (*). Higher molecular mass REC8-HA bands are indicated (**).
(B) ChIP enrichment (% input) from *REC8-HA rec8* and untagged wild-type (Col) flowers measured via qPCR at the *ATHILA*, *ATHILA6B*, and At2g02480 loci. Error bars show the SD.
(C) A representative region from chromosome 3 showing chromatin and recombination data (Table 2). Transposon (red) and gene (green) annotation are shown, with elements of interest highlighted by gray shading and labeled beneath.

(Figure 3A). These observations prompted us to investigate the relationship between recombination, chromatin, and REC8-HA ChIP enrichment at the fine scale.

REC8 Enrichment Associates with Suppression of Meiotic DSBs and Crossovers

REC8-HA enrichment peaks in ChIP-seq data were identified using the ranger tool within the PeakRanger suite, providing input library reads as a control for background (P ≤ 0.001 and false discovery rate [FDR] ≤ 0.01; Feng et al. 2011). This approach identified 86,386 REC8-HA peaks, which had a mean width of 444 bp (Supplemental Figure 2; Supplemental Tables 5 and 6). The average REC8-HA coverage profile between the peak start and end coordinates is positively correlated with nucleosome occupancy (r_s = 0.80) and anti-correlated with SPO11-1-oligos (r_s = −0.83), which was similar to the pattern observed when well-positioned nucleosomes (n = 57,734; mean width = 145 bp) were analyzed (Figure 4A). We analyzed REC8-HA peaks separately according to their location in the chromosome arms or pericentromeres and observed the same trends of nucleosome enrichment and SPO11-1-oligo depletion (Figure 4B). We next analyzed sets of 3320

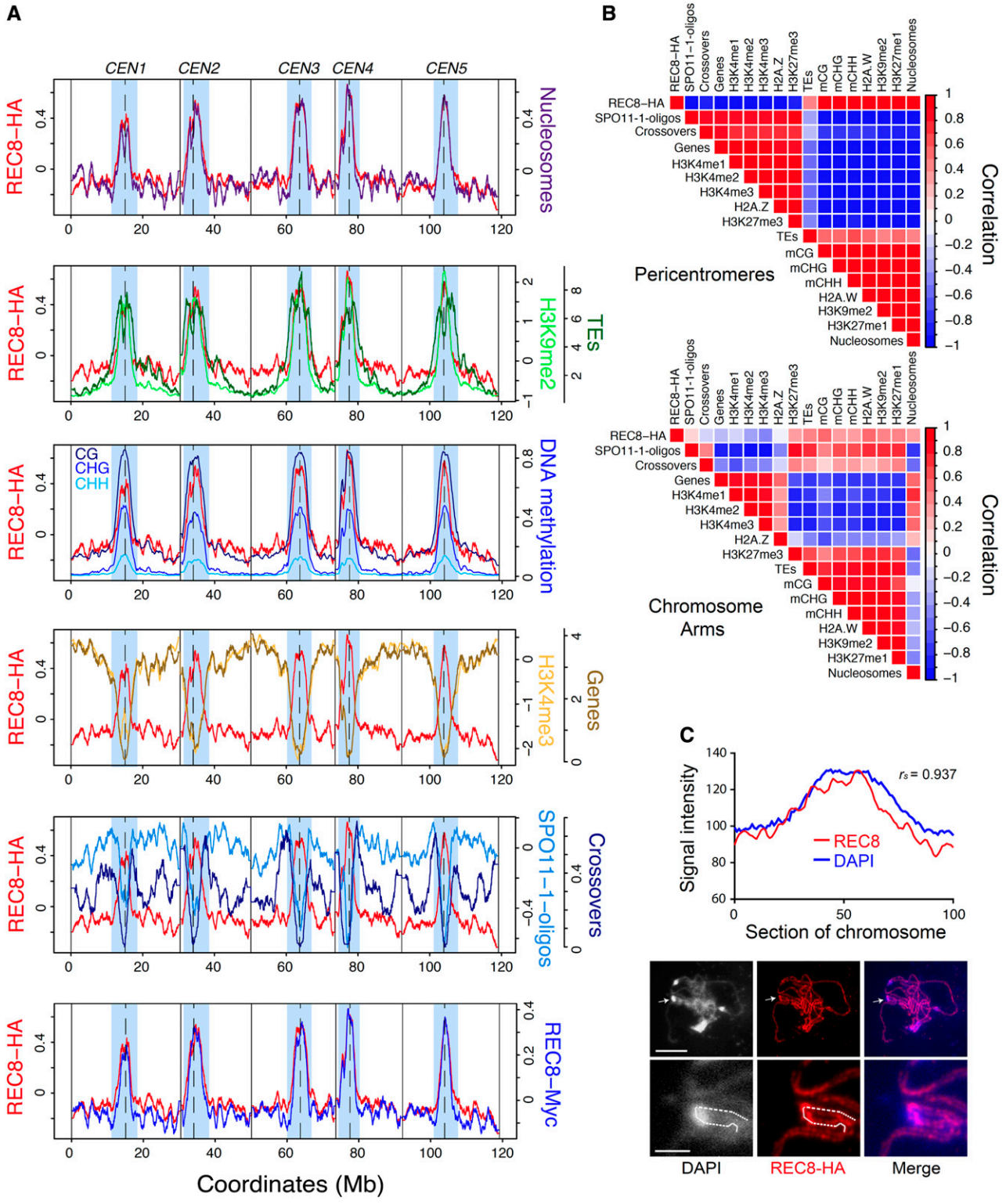

Figure 3. Genome-Wide Landscapes of REC8, Heterochromatin, Euchromatin, and Meiotic Recombination.

(A) Genome-wide profiles of REC8-HA (red, $\log_2$(ChIP/input)) and nucleosomes (purple, $\log_2$(MNase/gDNA)). Vertical solid lines indicate telomeres and dashed lines indicate centromeres, with the pericentromeres shaded in blue. Plots beneath compare REC8-HA (red) with TEs (dark green, TE/10 kb), H3K9me2 (green, $\log_2$(ChIP/input)), DNA methylation (blue, proportion methylated in CG, CHG and CHH contexts/200 kb; Stroud et al., 2013), genes (brown,

crossovers (mean resolved width = 976 kb) and 5914 SPO11-1-oligo hotspots and observed opposite trends to the REC8-HA peaks, with depleted nucleosomes and REC8-HA, compared with the same number of random windows with the same widths (Figure 4A; Choi et al., 2018; Serra et al., 2018). Hence, at the local scale, higher nucleosome and REC8 occupancy associate with suppression of both meiotic DSBs and crossovers.

REC8-HA peaks and SPO11-1-oligo hotspots were evaluated for overlap with other genomic features by performing permutation tests using the R package regioneR (Gel et al. 2016). For each test, 10,000 sets of randomly positioned loci with the same width distribution as the REC8-HA peaks or SPO11-1-oligo hotspots were defined. For each set, the number of random loci overlapping features of interest was then compared with the observed number of REC8-HA peaks or SPO11-1-oligo hotspots overlapping the features. This provides the basis for calculating an empirical P-value denoting the significance of the observed overlap (Supplemental Figure 2; Supplemental Tables 5 and 6). REC8-HA peaks overlapped with well-positioned nucleosomes and H3K9me2 peaks significantly more than expected by chance, whereas they overlapped SPO11-1-oligo hotspots and crossovers significantly less than expected (Supplemental Figure 2; Supplemental Tables 5 and 6). This provides statistical support for nucleosomes and REC8 colocalizing and exerting a suppressive effect on meiotic recombination.

DNA base composition is known to influence nucleosome positioning, meiotic recombination, and cohesin occupancy in multiple systems (Laloraya et al., 2000; Blat et al., 2002; Glynn et al., 2004; Choi et al., 2018). Therefore, we analyzed AT:GC content around REC8-HA peaks, well-positioned nucleosomes, SPO11-1-oligo hotspots, and crossovers (Figure 4C). Consistent with the known properties of nucleosomes (Segal and Widom, 2009), we observed pronounced depletion of AT and enrichment of GC bases around well-positioned nucleosomes (Figure 4C). Similarly, REC8-HA peaks show GC enrichment and AT depletion (Figure 4C), supporting the correlations between REC8-HA and nucleosome occupancy (Figures 4A and 4B). By contrast, both SPO11-1-oligo hotspots and crossovers show the opposite trends of AT enrichment and GC depletion (Figure 4C), as reported by Choi et al. (2018). This reveals that variation in DNA sequence frequency, chromatin structure, cohesin occupancy, and recombination are intimately connected in Arabidopsis, with GC richness underlying local nucleosome and REC8 enrichment and suppression of meiotic recombination.

REC8, Chromatin, and Recombination within TEs

We previously observed that Arabidopsis TE families are differentiated by levels of nucleosome occupancy and SPO11-1-oligos (Choi et al., 2018). For example, Gypsy, Copia, and LINE1 RNA transposons are relatively nucleosome dense and suppressed for SPO11-1-oligos, compared with DNA elements including MuDR and Helitron transposons that are nucleosome depleted, DSB active, and enriched in proximity to genes (Choi et al., 2018). We therefore compared REC8-HA levels in DNA versus RNA TEs and at the same number of randomly positioned loci of the same widths (Figures 5A and 5B). We observed that DNA elements were relatively depleted for REC8-HA and nucleosomes, whereas higher levels occurred in RNA elements (Figures 5A and 5B). This correlates with DNA elements showing lower levels of the heterochromatic marks H3K9me2 and CG, CHG, and CHH DNA methylation, compared with RNA transposons (Figures 5A and 5B).

We next evaluated overlap of REC8 peaks, well-positioned nucleosomes, and SPO11-1-oligo hotspots with different TE families (Figure 5C). Gypsy, LINE1, Copia RNA, and EnSpm/CACTA DNA transposons showed significant positive overlap with REC8 peaks and nucleosomes and negative overlap with SPO11-1-oligo hotspots (Figure 5C). By contrast, MuDR, HELITRON, and Pogo/Tc1/Mariner DNA transposons overlap REC8-HA and nucleosome peaks significantly less than expected by chance and SPO11-1-oligo hotspots significantly more than expected (Figure 5C). To illustrate differences in transposons, we show a representative region on chromosome 3 containing a REC8-enriched *COPIA81* RNA element, in the vicinity of a REC8-depleted *ATREP3* Helitron DNA element (Figure 5D). Hence, Arabidopsis transposon families are highly differentiated for REC8-cohesin enrichment, chromatin, and recombination.

REC8 Recruitment to Heterochromatin Is Unimpaired in *kyp suvh5 suvh6* H3K9me2 and non-CG DNA Methylation Mutants

Because of the enrichment of REC8 observed in the pericentromeres (Figure 2A), we sought to investigate whether loss of heterochromatic marks would change cohesin occupancy, as observed in fission yeast H3K9 methylation mutants (Bernard et al., 2001; Nonaka et al., 2002; Mizuguchi et al., 2014; Folco et al., 2017). Previously, we observed that *kyp suvh5 suvh6* triple mutants, which lose H3K9me2 and non-CG methylation, gain SPO11-1-oligos within heterochromatic sequences (Stroud et al., 2014; Underwood et al., 2018). Therefore, we repeated REC8-HA ChIP-seq in *kyp suvh5 suvh6* mutants. Floral buds from pooled F_3 plants were used for this experiment, derived from the same *REC8-HA* line crossed to *kyp suvh5 suvh6*. We also performed H3K9me2 ChIP-seq in *kyp suvh5 suvh6* to map the change of this chromatin modification. H3K9me2 and non-CG methylation are

Figure 3. (continued).

genes/10 kb), H3K4me3 (yellow, $\log_2$(ChIP/input)), SPO11-1-oligos (light blue, $\log_2$(oligos/gDNA)), crossovers (dark blue, crossovers/10 kb), and REC8-Myc (blue, $\log_2$(ChIP/input)).

(B) Correlation matrices showing genome-wide r_s for the indicated parameter pairs, with cells color coded according to the correlation scale shown to the right.

(C) REC8-HA (red) and chromatin (blue/white, DAPI) were costained on pachytene stage chromosomes, and 20 axis sections of 100 pixels centered on heterochromatin were used to quantify signal intensity (arbitrary units). A representative full cell image is shown beneath. Scale Bar = 10 μm. Arrows indicate the area of the cell used for the close-up image beneath; the dashed line indicates the section of chromatin used for analysis. Scale Bar = 2.5 μm.

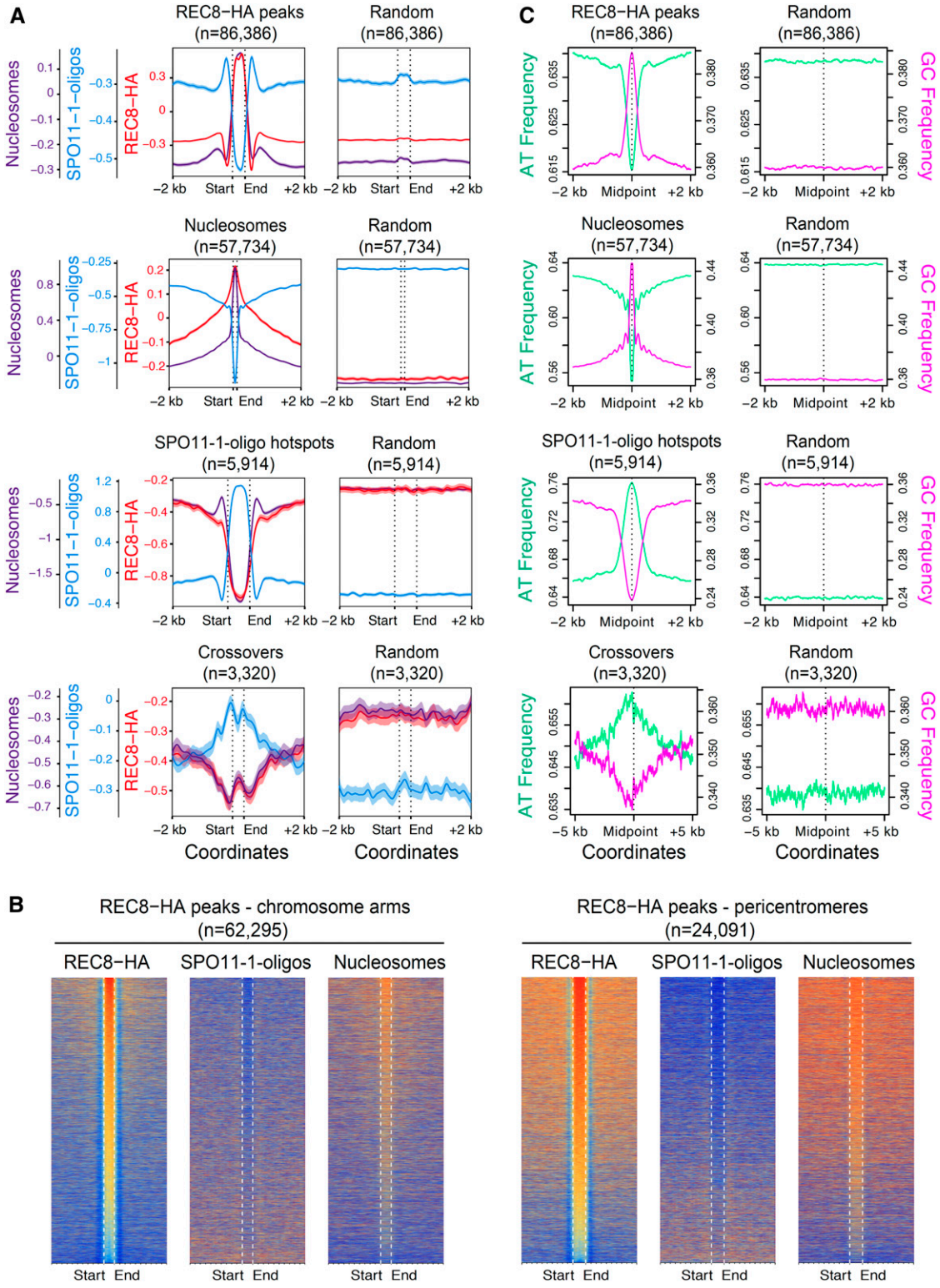

Figure 4. REC8-HA and Nucleosome Enrichment Correlate with Suppression of Meiotic Recombination at the Fine Scale.

(A) Mean coverage profiles for REC8-HA (red, $\log_2$(ChIP/input)), SPO11-1-oligos (blue, $\log_2$(oligos/gDNA)), and nucleosomes (purple, $\log_2$(MNase/gDNA)) within REC8-HA peaks and 2-kb flanking regions, or the same number of random positions of the same widths. Plots are repeated for well-positioned nucleosomes, SPO11-1-oligo hotspots, and crossovers (5-kb flanking regions). Plot ribbons denote 95% confidence intervals for windowed values.

tightly coupled in Arabidopsis, and both marks are lost in *kyp suvh5 suvh6* mutants (Figure 6A; Stroud et al., 2014).

In contrast to fission yeast, we observed that the pattern of REC8-HA enrichment along the chromosomes in *kyp suvh5 suvh6* was highly similar to that of the wild type, with strong enrichment observed in proximity to the centromeres (Figure 6A). We immunostained for REC8-HA in the wild-type and *kyp suvh5 suvh6* male meiocytes and observed that normal signal intensity with the heterochromatic chromocenters was maintained, using the F_3 lines generated for ChIP analysis (Figure 6B). Finally, we analyzed male meiocytes in *kyp suvh5 suvh6* cytologically for phenotypes associated with *rec8* mutants (Figure 6C; Bhatt et al., 1999; Cai et al., 2003; Chelysheva et al., 2005). At pachytene stage, normal paired axes are observed in *kyp suvh5 suvh6* and sister chromatid cohesion is maintained at metaphase I and metaphase II, without obvious defects in chromosome segregation (Figure 6C). Hence, REC8-cohesin is recruited to levels sufficient to maintain sister chromatid cohesion and bivalent formation during meiosis in *kyp suvh5 suvh6*.

Transcription Influences REC8 Occupancy within Genes and Transposons

Transcription has been shown to shape mitotic and meiotic cohesin occupancy (Lengronne et al., 2004; Mizuguchi et al., 2014; Sun et al., 2015). Therefore, we analyzed REC8-HA enrichment in relation to gene bodies (transcription start site [TSS]-transcription termination site [TTS]) and 2 kb of flanking sequences, versus the same number of randomly positioned loci of the same widths (Figure 7A). As reported, SPO11-1-oligos are depleted within gene bodies and show greatest enrichment in nucleosome-free regions in promoters and terminators (Figure 7A; Choi et al., 2018). By contrast, REC8-HA, MNase-seq (nucleosomes), and RNA-seq signal are enriched intragenically, and their average profiles show positive correlations with one another (r_s = 0.66 to 0.96), with highest signal toward gene 3′ ends (Figure 7A). For example, REC8-HA is relatively depleted from the 5′ regions of genes that show greatest enrichment of H2A.Z and H3K4me3 (Figure 7A). These correlations indicate that transcription may influence both nucleosome and REC8 occupancy within gene bodies, or vice versa.

To explore the relationship with transcription, we ordered genes by increasing expression measured from floral RNA-seq data and compared this with REC8-HA ChIP-seq enrichment within genes (Figure 7B). This showed a negative correlation between REC8-HA occupancy within genes and expression level ($r_s = -0.40$; Figure 7B). As gene expression increases, REC8-HA and nucleosomes occur at lower levels intragenically and show an increased bias toward the gene 3′ ends (Figure 7B). This is consistent with higher RNA polymerase activity causing migration of cohesin in the direction of transcription. Genes with higher expression also show greater enrichment of H3K4me3 and H2A.Z at their 5′ end, coincident with lower local REC8-HA levels (Figure 7B). Interestingly, SPO11-1-oligos in gene promoters and terminators did not significantly correlate with gene expression or intragenic levels of REC8-HA (Figure 7B).

We performed RNA-seq from wild-type and *kyp suvh5 suvh6* meiotic-stage flowers and identified 179 TEs that showed significant upregulation of expression in the triple mutant. Upregulated transposons were enriched for elements belonging to the EnSpm (hypergeometric test, $P = 1.77 \times 10^{-25}$), Copia ($P = 1.69 \times 10^{-17}$), Harbinger ($P = 0.0004$), and LINE1 ($P = 0.0125$) superfamilies (Supplemental Table 7). Upregulated Copia transposons ($n = 45$) show loss of H3K9me2 and non-CG DNA methylation in *kyp suvh5 suvh6* (Figure 7C). As a control, we compared upregulated Copia elements with the same number of randomly selected Copia elements that did not show a significant change of expression in *kyp suvh5 suvh6* (non-differentially expressed), or to the same number of randomly positioned loci of the same widths (Figure 7C). The upregulated Copia transposons showed regions with significant gain of SPO11-1-oligos in *kyp suvh5 suvh6* compared to the wild type, which overlapped with regions of significant REC8 depletion, close to the transposon promoters (Benjamini–Hochberg-adjusted Mann–Whitney–Wilcoxon [MWW] $P < 0.1$; Figure 7C). No significant differences in SPO11-1-oligos or REC8 were detected in the Copia transposons that were not upregulated (Figure 7C). This is consistent with changes to chromatin and transcription at these transposons associating with modifications to REC8 occupancy and DSB levels.

Abnormal Chromosome Axis Structures Form in *rec8* That Recruit the Homologous Recombination Machinery

Finally, we sought to explore the consequences of *rec8* mutation for meiotic chromosome architecture and recombination at the cytological level. We used epifluorescence immunocytology and structured illumination microscopy to analyze the axis proteins ASY1 and ASY3 in *rec8*. In the wild type, ASY1 and ASY3 colocalize along linear axes from leptotene until zygotene (Figures 8A to 8D; Ferdous et al., 2012). In *rec8*, ASY1 and ASY3 occurred in abnormal structures that persisted throughout mid-prophase I (Figures 8A to 8D), as reported by Chelysheva et al. (2005). The length of chromosome axis structures stained by ASY1 in *rec8* was significantly shorter compared to the wild type at leptotene (mean = 30 μm versus 220 μm; MWW test, $P = 3.02 \times 10^{-11}$; Figure 8D; Supplemental Table 8).

We analyzed the SC component ZYP1 in the wild type and *rec8* (Figures 8A and 8B). Chromosome synapsis initiates at zygotene in the wild type, with the formation of ZYP1 stretches that become

Figure 4. (continued).

(B) Heatmaps of REC8-HA ($\log_2$(ChIP/input)), SPO11-1-oligos ($\log_2$(oligos/gDNA)), and nucleosomes ($\log_2$(MNase/gDNA)) within REC8-HA peaks and 2-kb flanking regions, with peaks (rows) ordered by descending REC8-HA values. Analysis was repeated according to peak locations in the chromosome arms (left) or pericentromeres (right).

(C) Plots as for **(A)** but analyzing DNA base frequencies (AT, green; GC, pink) across the same regions in 4- or 10-kb regions around feature midpoints.

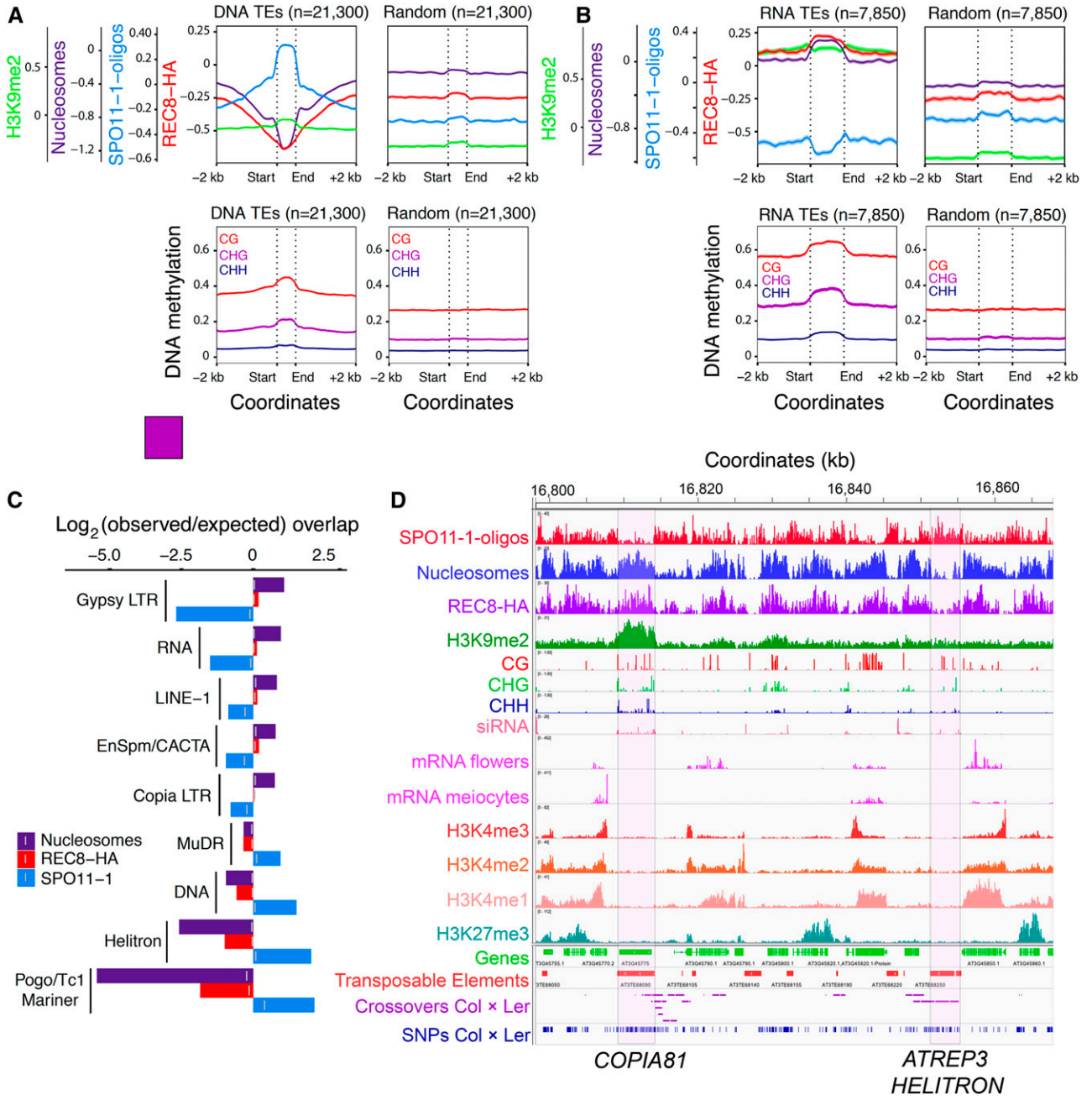

Figure 5. REC8, Chromatin, and Recombination within Arabidopsis TE Families.

(A) REC8-HA (red, $\log_2$(ChIP/input)), SPO11-1-oligos (blue, $\log_2$(oligos/gDNA)), nucleosomes (purple $\log_2$(MNase/gDNA)), and H3K9me2 (green, $\log_2$(ChIP/input)) within DNA transposons and 2-kb flanking regions, or the same number of random positions of the same widths. The mean width of the elements is indicated by vertical dashed lines. Beneath are plots analyzing the same transposons for mean DNA methylation proportion in CG (red), CHG (purple), and CHH (blue) sequence contexts. Plot ribbons denote 95% confidence intervals for windowed mean coverage or DNA methylation proportion.
(B) As for **(A)** but analyzing RNA transposons.**C)** Bar graphs showing permutation-test derived $\log_2$(observed/expected) overlap of REC8-HA peaks (red), SPO11-1-oligo hotspots (blue), or nucleosomes (purple) with the indicated transposon superfamilies. Vertical gray lines mark significance thresholds ($\alpha = 0.05$).
(D) A representative region from chromosome 3 showing chromatin, recombination, and genome annotation (Table 2). Transposon (red) and gene (green) annotation are shown, with transposons of interest labeled and highlighted by gray shading.

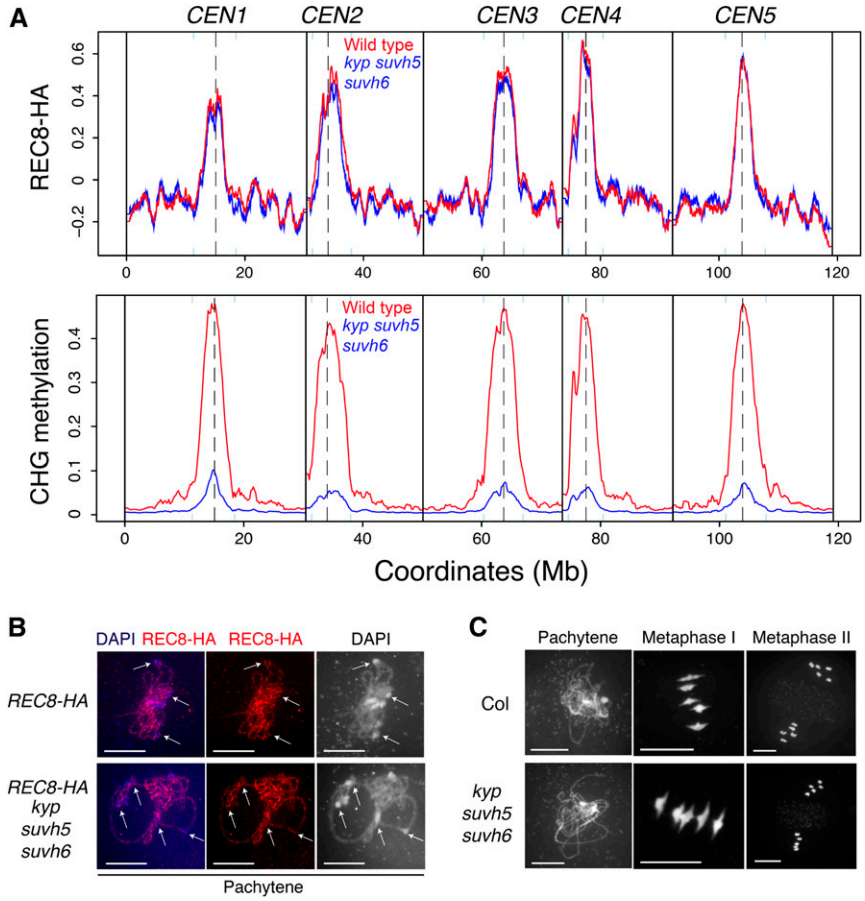

Figure 6. REC8 Occupancy in Heterochromatin Is Maintained in *kyp suvh5 suvh6*.

(A) Genome-wide profiles of REC8-HA ($\log_2$(ChIP/input)) from the wild type (red) and *kyp suvh5 suvh6* (blue). CHG context DNA methylation proportion from the wild type (red) and *kyp suvh5 suvh6* (blue) are plotted beneath. Vertical solid lines indicate telomeres and dotted lines indicate centromeres.
(B) Male meiocytes of the wild type (Col) and *kyp suvh5 suvh6* were immunostained for REC8-HA (red) and stained for DNA (DAPI, blue) at pachytene stage. White arrows indicate DAPI-dense chromocenters. All scale bars = 10 μm.
(C) DAPI-stained spreads of wild type (Col) and *kyp suvh5 suvh6* male meiocytes at the labeled stages of meiosis.

depleted of ASY1 (Figure 8A), until full synapsis is achieved at pachytene (Lambing et al., 2015). We observed short stretches of ZYP1 polymerization between the abnormal ASY1 axis structures in *rec8* (Figures 8A and 8B). In the wild type, ZYP1 polymerizes between axes separated by a mean distance of 109 nm (Figure 8B; Supplemental Table 9). In *rec8*, ZYP1 was detected between ASY1 axis structures with a mean distance not significantly different from that of the wild type (119 nm; MWW test, P = 0.22; Figures 8B and 8D; Supplemental Table 9). PCH2 is a conserved meiotic AAA+ATPase required to remodel the axis during synapsis, which forms a linear signal with ZYP1 at pachytene (Figure 8E; Lambing et al., 2015). The *rec8* axis structures costained for both PCH2 and ZYP1 (Figure 8E). Interestingly, the SMC3 cohesin subunit was also recruited to the ASY1 axis structures, despite the absence of REC8 (Figure 8F). Therefore, *rec8* abnormal axial structures include ASY1, ASY3, and SMC3 and can recruit PCH2 and ZYP1 to produce synapsed structures with a similar inter-axis width to the wild type.

To visualize meiotic DSBs, we immunostained for γH2A.X and ASY1 and observed a mean of 202 axis-associated foci in the wild type (Figures 9A and 9C; Supplemental Table 10). In *rec8*, γH2A.X foci were significantly reduced (mean = 53; MWW test, $P = 3.37 \times 10^{-6}$), although they remained associated with the ASY1 axis structures (Figures 9A and 9C). We also immunostained for the single-stranded DNA binding proteins RAD51, RPA1a, and DMC1 that show mean axis-associated foci numbers of 181, 174, and 172, respectively, at mid-prophase I in the wild type, numbers that were significantly reduced in *rec8* to 39, 36, and 14 (MWW test, $P = 3.37 \times 10^{-6}$, $P = 3.33 \times 10^{-6}$, $P = 1.08 \times 10^{-5}$; Figures 9A and 9C; Supplemental Tables 10 and 11). Positive correlations exist between axis length and γH2A.X and RAD51 foci per nuclei, in both the wild type and *rec8* ($r_s = 0.83$ and 0.69 and $r_s = 0.92$ and 0.77, respectively; Figure 9D; Supplemental Table 12), which is consistent with a requirement of the axis for DSB formation. This provides cytological evidence that DSB formation and interhomolog strand invasion are associated with abnormal axial structures in *rec8* mutants.

Finally, we immunostained for DNA repair factors required for formation of interfering crossovers. In the wild type, the MutS

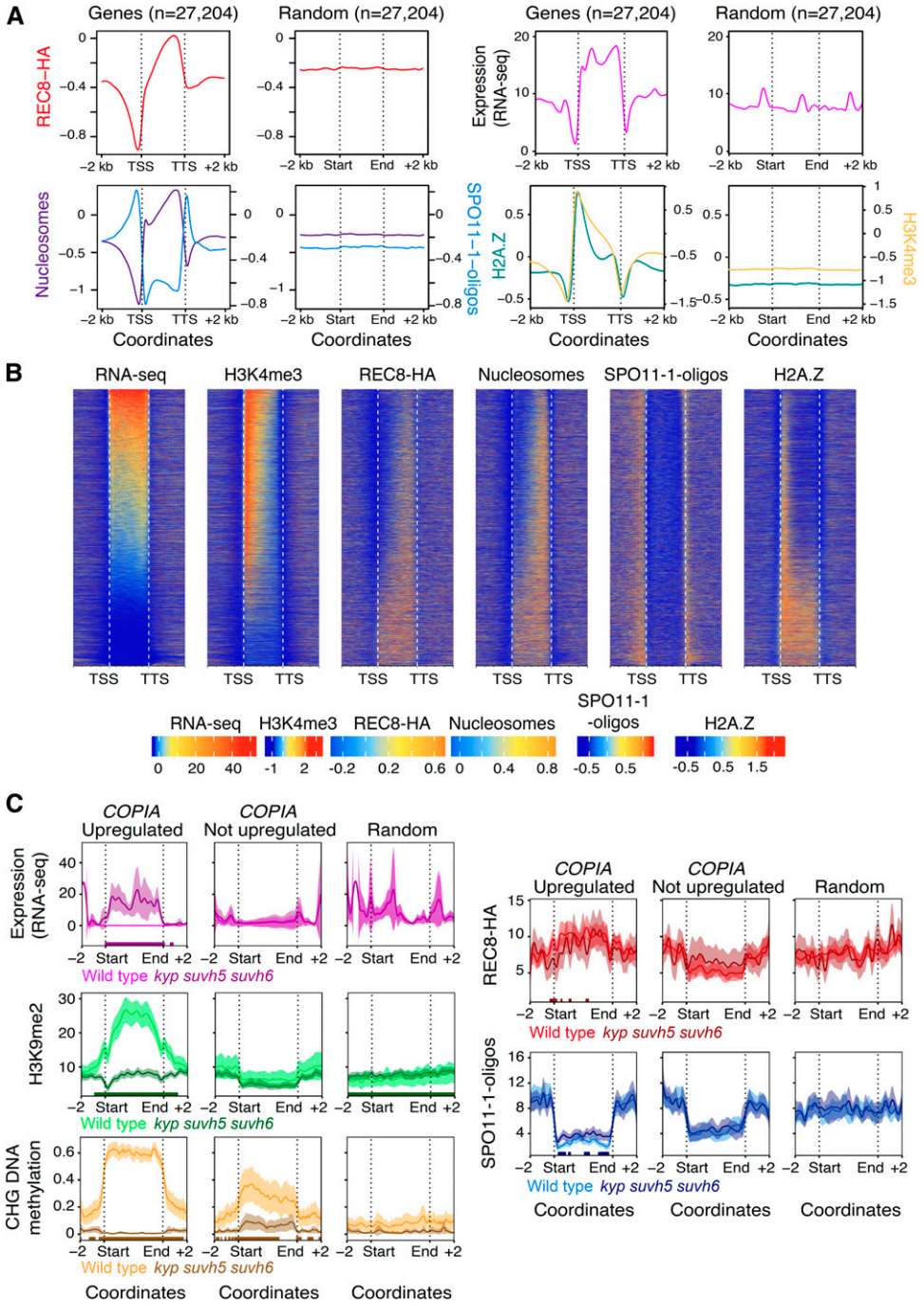

Figure 7. Transcription Shapes REC8 Occupancy.

(A) Mean coverage profiles for REC8-HA (red, $\log_2$(ChIP/input)) between gene TSS and TTS and 2-kb flanking regions, or the same number of random regions of the same widths. Also plotted are SPO11-1-oligos (blue, $\log_2$(oligos/gDNA)), nucleosomes (purple, $\log_2$(MNase/gDNA)), RNA expression (pink, RNA-seq normalized by total coverage), H2A.Z (turquoise, $\log_2$(ChIP/input)), and H3K4me3 (yellow, $\log_2$(ChIP/input)).
(B) Heatmaps of REC8-HA, nucleosomes, SPO11-1-oligos, RNA-seq, H3K4me3, and H2A.Z within genes and 2-kb flanking regions. Rows have been ordered by decreasing RNA-seq within genes.
(C) Mean profiles in the wild type and *kyp suvh5 suvh6* for RNA-seq (purple), H3K9me2 (green, ChIP), CHG DNA methylation (yellow), REC8-HA (red), and SPO11-1-oligos (blue) within Copia transposons that are upregulated in *kyp suvh5 suvh6*, or a random subset of those that are not, or the same number of random positions of the same widths. Plot ribbons denote 95% confidence intervals for the windowed mean coverage or DNA methylation proportion values. Windows showing significant changes in *kyp suvh5 suvh6* (with Benjamini–Hochberg-adjusted MWW $P < 0.1$) are indicated by colored ticks along the *x* axis.

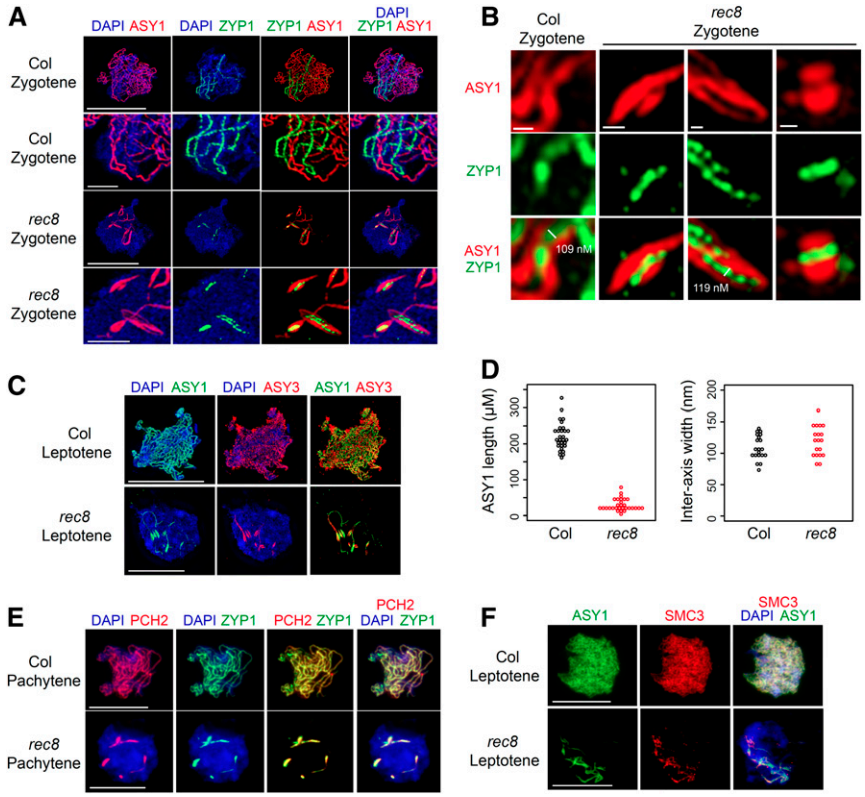

Figure 8. Abnormal Axis Structures in *rec8* Undergo Synapsis.

(A) Structured illumination microscopy images of wild-type (Col) and *rec8* male meiocytes at zygotene stage, stained for ASY1 (red), ZYP1 (green), and chromatin (DAPI, blue). Bars = 10 μm. Close-ups of synapsed regions are shown for each genotype, where scale bars = 2.5 μm.
(B) As for **(A)** but showing synapsed regions stained with ASY1 (red) and ZYP1 (green) in the wild type (Col) and *rec8*, with inter-axis distance indicated in white. Bars = 200 nm.
(C) As for **(A)** but at leptotene stage and staining for ASY1 (green), ASY3 (red), and chromatin (DAPI, blue).
(D) Quantification of ASY1 axis length (μm) and inter-axis width (nm) in the wild type (black) and *rec8* (red).
(E) As for **(A)** but pachytene stage cells stained for PCH2 (red), ZYP1 (green), and chromatin (DAPI, blue).
(F) As for **(A)** but at leptotene stage and stained for ASY1 (green), SMC3 (red), and chromatin (DAPI, blue). Scale Bars =10 μm.

homolog MSH4 forms a mean of 179 axis-associated foci at leptotene that were significantly reduced in *rec8* (mean = 13 foci; MWW test, $P = 1.10 \times 10^{-5}$) and to a greater extent than observed for DSB foci (Figures 9A and 9C; Supplemental Tables 10 and 11). The MutL homolog MLH1 acts in late prophase I and shows a mean of 10.4 chiasma-associated foci at diakinesis, which were significantly reduced in *rec8*, yet remained associated with chromatin (mean = 4.9 foci; MWW test, $P = 2.59 \times 10^{-10}$; Figure 9C; Supplemental Table 13). Therefore, although *rec8* abnormal axis structures recruit recombination foci, they are reduced in number relative to the wild type. Together, these cytological data support a role for REC8-cohesin in organizing correct polymerization of the axis and SC to promote high-fidelity interhomolog recombination.

DISCUSSION

At the chromosome scale, we observe the greatest REC8 ChIP-seq enrichment in proximity to the centromeres and within pericentromeric heterochromatin. This parallels elevated REC8 enrichment observed in budding and fission yeast centromeres (Kugou et al., 2009; Ito et al., 2014; Sun et al., 2015; Folco et al., 2017). In contrast to these species, Arabidopsis possesses megabase-scale centromeres, consisting of *CEN180* satellite repeats, a subset of which bind to the centromeric CENH3 histone variant (Tables 1 to 3; Zhang et al., 2008; Maheshwari et al., 2017). The *CEN180* repeats are surrounded by repetitive heterochromatin enriched in Gypsy, Copia, and EnSpm TEs, which are epigenetically modified by DNA methylation, H3K9me2, and H2A.W (Stroud et al., 2014; Yelagandula et al., 2014). We previously observed that SPO11-1-oligos increase within heterochromatin in *kyp suvh5 suvh6* H3K9me2/non-CG DNA methylation mutants (Underwood et al., 2018). Here, we show that REC8 is still effectively loaded in the centromeric regions in *kyp suvh5 suvh6*. In fission yeast, which possesses complex regional centromeres, loss of centromeric H3K9me2 in *clr4* mutants greatly decreases REC8 loading and causes defects in chromosome segregation (Bernard et al., 2001; Nonaka et al., 2002; Ellermeier et al., 2010; Folco et al., 2017). Hence, in this respect Arabidopsis more closely resembles mouse *suv39h1 suv39h2* H3K9me2

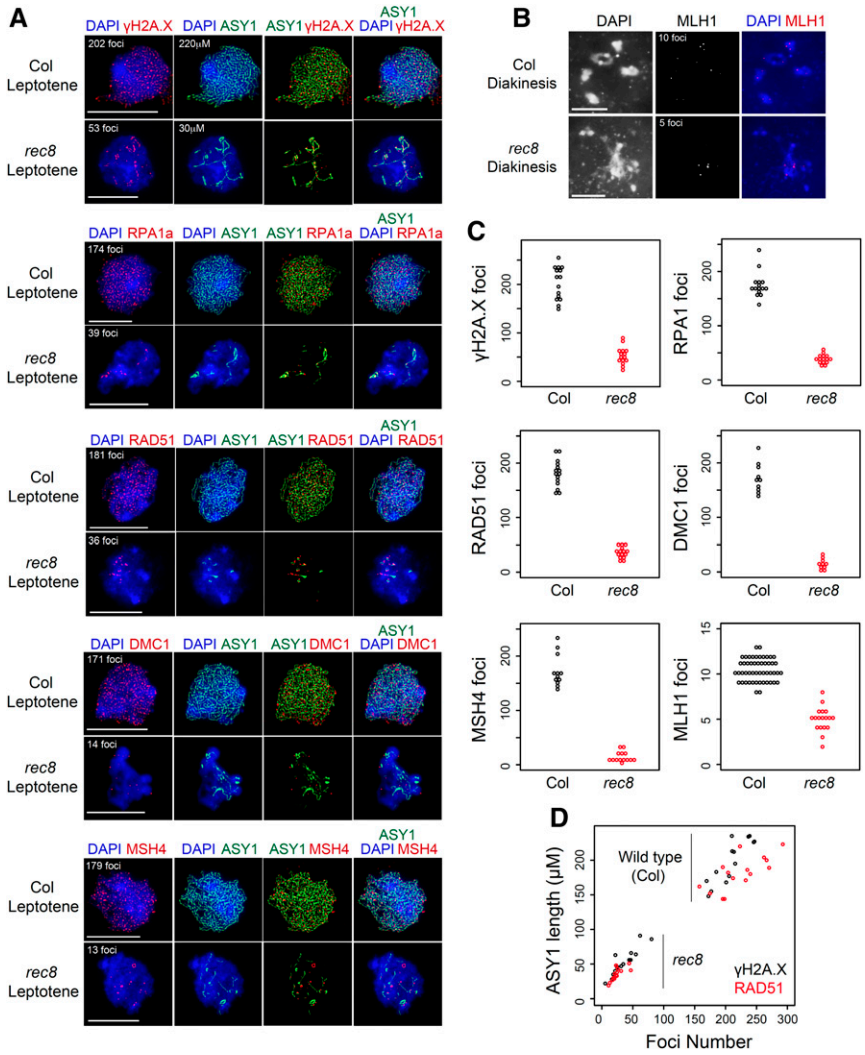

Figure 9. Abnormal Axis Structures in *rec8* Recruit DSB and Crossover Foci.

(A) Wild-type (Col) and *rec8* male meiocytes at leptotene stage were stained for ASY1 (green), γH2A.X (red), and DNA (DAPI, blue). Also shown are male meiocytes stained for RPA1a, RAD51, DMC1, MSH4 (all red), and ASY1 (green).
(B) Diakinesis-stage meiocytes from the wild type and *rec8* stained for MLH1 (red) and DNA (DAPI, blue). All scale bars = 10 μm.
(C) γH2A.X, RPA1a, RAD51, DMC1, MSH4, and MLH1 foci number measured in the wild type (black) and *rec8* (red).
(D) Plot of ASY1 axis length (μm) against foci number of γH2A.X (black) and RAD51 (red) in wild-type and *rec8* meiocytes.

mutants, where mitotic cohesin is recruited to heterochromatin but with remodeling on major versus minor satellite repeats (Guenatri et al., 2004; Koch et al., 2008). Therefore, it is possible that other heterochromatic marks, including CG DNA methylation, H3K27me1, or H2A.W (Jacob et al., 2009; Stroud et al., 2013; Stroud et al., 2014; Yelagandula et al., 2014), or other features of the centromere including the kinetochore (Hinshaw et al., 2017), could play important roles in REC8 loading in the Arabidopsis centromeres and pericentromeric heterochromatin.

We observe a strong correlation between REC8 enrichment and nucleosome occupancy (measured via MNase-seq) across the genome. In this respect, it is notable that in vitro binding experiments testing the mobility of a fission yeast cohesin complex (Psm1, Psm3, Psc3, Rad21) along a single tethered DNA molecule showed hindrance caused by the presence of nucleosomes (Stigler et al., 2016). Hence, it is possible that Arabidopsis nucleosomes restrict REC8-cohesin mobility, contributing to the observed correlations. In budding yeast, the Scc2/Scc4 complex functions to load cohesin within nucleosome-free gene promoter regions, with cohesin then migrating in the direction of transcription toward gene terminator regions (Lengronne et al., 2004), which is also evident for REC8-cohesin during meiosis (Sun et al., 2015), and during fission yeast mitosis (Schmidt et al., 2009). In mouse cells, the absence of CTCF leads to accumulation of cohesin at the 3′ ends of transcribed genes (Busslinger et al., 2017). In Arabidopsis, we observe a negative relationship with transcription level and REC8 occupancy, with higher levels of transcription associating with a 3′ bias in REC8 enrichment, although

we do not observe REC8 accumulation in gene terminators. By contrast, Arabidopsis terminators are nucleosome depleted and enriched for meiotic DSBs (Choi et al., 2018), unlike in budding yeast where SPO11-1-oligo hotspots occur at promoters and not at terminators (Pan et al., 2011). Hence, although a conserved role for transcription patterning cohesin occupancy is apparent, the relative locations of REC8 enrichment and DSBs with respect to gene architecture vary between genomes. It is also important to consider that plant heterochromatin is actively transcribed by Pol IV and Pol V RNA polymerases, which produce short transcripts required for RNA-directed DNA methylation (Law and Jacobsen, 2010). Hence, it will also be interesting to explore the effects of heterochromatic transcription on cohesin occupancy in plants in the centromere proximal regions.

We show that REC8 occupancy is associated with multiple chromatin states within the Arabidopsis genome in both gene- and repeat-rich regions. We show significant differentiation of DNA versus RNA transposon occupancy by REC8, which correlates with chromatin and meiotic DSB levels. At both the chromosome and fine scales, REC8 enrichment associates with suppression of meiotic DSBs and crossovers. This is consistent with anchoring of chromatin loops to the axis via REC8-cohesin causing local exclusion of the recombination machinery. Cohesin has a role in DSB repair and can antagonize interhomolog recombination by promoting inter-sister repair of DSBs (Hong et al., 2013; da Costa-Nunes et al., 2014; Yoon et al., 2016; Bolaños-Villegas et al., 2017). Hence, in Arabidopsis it is also possible that high levels of REC8 associate with promotion of inter-sister repair, which could contribute to the low crossover frequency observed in the heterochromatic pericentromeres. Despite the local suppressive effect on recombination, REC8 is also required to establish an organized meiotic chromosome architecture and in its absence catastrophic recombination occurs, leading to chromosome fragmentation (Bhatt et al., 1999; Cai et al., 2003; Chelysheva et al., 2005). We show that in the absence of REC8, axis proteins undergo polymerization into disorganized structures that nevertheless recruit foci associated with DSB formation and repair and form regions of SC. We propose that a subset of these repair foci represent illegitimate interhomolog recombination events that cause chromosome fragmentation at metaphase I. In conclusion, we show that chromatin, the axis, and REC8-cohesin play tightly integrated roles organizing meiotic chromosome architecture and recombination during Arabidopsis meiosis.

METHODS

Plant Materials

Arabidopsis (*Arabidopsis thaliana*) plants were grown on commercial F2 compost in controlled environment chambers under the following conditions: 60% humidity and long-day conditions (16-h-light/8-h-dark cycle) with 150-μmol light intensity using light-emitting diode bulbs with standard NS1 spectrum and at 20°C. The following mutant alleles in the Col accession were used: *rec8-1* (Salk_091193) was used for cytological experiments (Ferdous et al., 2012) and *rec8-3* (SAIL_807_B08) was used for transformation with epitope-tagged *REC8-HA* and *REC8-Myc* transgenes (d'Erfurth et al., 2009). The *kyp suvh5 suvh6* triple mutant (SALK_041474, GK-263C05, SAIL_1244_F04) was obtained from Steven Jacobsen (University of California, Los Angeles).

Cytological Analysis of Meiosis

Fixation of Arabidopsis inflorescences from pools of Col, *rec8-1*, or *REC8-HA*/*Myc* plants and chromosome spreads of pollen mother cells were performed, as described by Ross et al. (1996). Immunostaining of MLH1, REC8-HA, and REC8-Myc was performed on acetic acid chromosome spreads using fixed inflorescences, as described by Chelysheva et al. (2010). Chromosome spreads of Arabidopsis pollen mother cells and immunostaining of ASY1, γH2A.X, RAD51, RPA1a, DMC1, MSH4, ASY3, SMC3, PCH2, and ZYP1 were prepared using fresh buds from pools of Col or *rec8-1* plants, as described by Armstrong et al. (2002). The following antibodies were used: α-ASY1 (rat/rabbit, 1:500 dilution; Armstrong et al., 2002), α-ZYP1 (rat/rabbit, 1:500 dilution; Higgins et al., 2005), α-γH2A.X (Ser 139; Merck catalog no. 07-164, 1:100 dilution; Ferdous et al., 2012), α-RAD51 (rabbit, 1:500 dilution; Sanchez-Moran et al., 2007), α-DMC1 (rabbit, 1:500 dilution; Sanchez-Moran et al., 2007), α-MSH4 (rabbit, 1:500 dilution; Higgins et al., 2004), α-RPA1a (rabbit, 1:500 dilution; Osman et al., 2009), α-ASY3 (rabbit, 1:500 dilution; Ferdous et al., 2012), α-MLH1 (rabbit, 1:200 dilution; Chelysheva et al., 2010), α-SMC3 (rabbit, 1:500; Ferdous et al., 2012), α-PCH2 (rabbit, 1:500 dilution; Lambing et al., 2015), α-Myc (mouse, 1:50 dilution; 9E10 sc-40, Santa Cruz Biotechnology), and α-HA (rabbit, 1:250 dilution; ab9110, Abcam). Fluorescence in situ hybridization was performed on chromosome spreads of metaphase nuclei using *CEN180* probes, as described by Armstrong et al. (2001). Microscopy was conducted using a DeltaVision Personal DV microscope (Applied Precision/GE Healthcare) equipped with a charge-coupled device CoolSNAP HQ2 camera (Photometrics). Image capture was performed using SoftWoRx software version 5.5 (Applied Precision/GE Healthcare). Image analysis and processing were performed using ImageJ.

Generation of *REC8-3×HA and REC8-5×Myc* Transgenic Lines

The *REC8* locus was PCR amplified from Col genomic DNA, and 3×HA or 5×MYC epitopes were introduced at the stop codon. For each of the constructs, a genomic fragment containing 2.6 kb upstream of the *REC8* 5′ untranslated region was amplified using the primers REC8-tag_F and REC8-tag_R (Supplemental Table 14). A linker coding for the amino acids (GGGS)×4 was introduced between the last codon of the genomic sequence and the HA and Myc tags. A *Nos* terminator was introduced at the end of the HA and Myc tags. Tagged *REC8* genomic fragments were cloned into the pPZP211 binary vector using *Hind*III and *Sal*I restriction sites and used to transform *rec8-3* heterozygous plants using *Agrobacterium tumefaciens* strain GV3101. Primary transformants were selected on kanamycin supplemented Murashige and Skoog medium. The presence of transgenes in *rec8-3* homozygous backgrounds was confirmed by PCR genotyping.

Immunoprecipitation and Immunoblotting of Epitope-Tagged REC8

Unopened flower buds were collected from pools of Col, *REC8-HA rec8*, or *REC8-Myc rec8* F_3 plants. For each genotype, 1 g of unopened flower buds was ground in liquid nitrogen and transferred to lysis buffer (25 mM Hepes-NaOH, pH 7.9, 5 mM EDTA, 2% [v/v] SDS, 1 mM phenylmethylsulfonyl fluoride [PMSF], 2 mM DTT, and 1× protein cocktail inhibitor [11873580001, Roche]) and incubated for 20 min at 95°C. The solution was centrifuged at 17,000*g* for 20 min at 4°C. The supernatant was diluted with 3 volumes of dilution buffer (14 mM Tris, pH 8.0, 1% [v/v] Triton X-100, and 150 mM NaCl). For immunoprecipitation, 4 μg of α-HA (ab9110, Abcam) or α-Myc (ab9132, Abcam) antibodies was used per 0.25 g of buds, which were bound to Protein G Dynabeads (10004D, Invitrogen). The reaction was incubated for 16 h at 4°C and then washed four times with wash buffer (14 mM Tris, pH 8.0, 1% [v/v] Triton X-100, and 150 mM NaCl). Immunoprecipitated proteins were eluted from the beads by incubation with

1× SDS loading buffer for 5 min at 75°C. The eluted solution was used for immunoblotting.

Protein extracts and eluted proteins were loaded with 1× SDS loading buffer on a NuPage 3 to 8% (v/v) Tris acetate gel (EA0375BOX, Invitrogen). After proteins were separated through the gel using electrophoresis, proteins were transferred to a polyvinylidene fluoride membrane (162-0177, Bio-Rad) in transfer solution (25 mM Tris base, 192 mM Gly, and 20% [v/v] methanol, pH 8.3) for 1 h at 100 mV at 4°C. After transfer, the membrane was rinsed with TBST (20 mM Tris base and 150 mM NaCl, pH 7.6) and incubated in blocking buffer (5% [w/v] nonfat dried milk in TBST) overnight at 4°C with shaking. The membrane was then washed once for 15 min and twice for 5 min with TBST at room temperature. A solution of primary antibody diluted in blocking buffer was added (α-HA [ab9110, lot GR3231414, Abcam], 1/15,000 dilution; α-Myc [ab9132, lot GR254156, Abcam], 1/5000 dilution), and the membrane was incubated for 2 h at room temperature. The membrane was washed once for 15 min and then twice for 5 min with TBST. A solution of secondary antibody diluted in blocking buffer (α-HA [α-rabbit IgG–horseradish peroxidase, sc-2054, Santa Cruz Biotechnology], 1/20,000 dilution; α-Myc [α-goat IgG–horseradish peroxidase, sc-2768, Santa Cruz Biotechnology], 1/5000 dilution) was added, and the membrane was incubated for 1 h at room temperature. The membrane was washed once for 15 min and twice for 5 min with TBST at room temperature. The signal was detected on film with ECL Prime Western Blotting detection reagents (RPN2232, GE Healthcare) using a Xograph compact X4.

ChIP-Seq of Histone Modifications

Unopened flower buds were collected from pools of Col or *kyp suvh5 suvh6* plants. Two grams of unopened floral buds was used to perform ChIP-seq for H3K4me1, H3K4me2, H3K9me2, H3K27me1, and H3K9me2 in Col or *kyp suvh5 suvh6*, as described previously (Choi et al., 2018). Five micrograms of antibodies was used per gram of tissue. The following antibodies were used: α-H3K4me1 (catalog no. ab8895, lot GR312093, Abcam), α-H3K4me2 (catalog no. ab7766, lot GR289627, Abcam), α-H3K9me2 (catalog no. ab1220, lot GR244373, Abcam), and α-H3K27me1 (catalog no. 07-448, lot 2,869,720, Merck).

ChIP and Sequencing of REC8

Unopened flower buds were collected from pools of Col, *kyp suvh5 suvh6*, *REC8-HA rec8*, or *REC8-Myc rec8* F_3 plants. Ten grams of unopened floral buds was ground in liquid nitrogen and used to perform ChIP-seq for REC8-HA in the wild type (two biological replicates representing two independent collections of flower buds from pools plants) and *kyp suvh5 suvh6* (two biological replicates representing two independent collections of flower buds from pools plants) and for REC8-Myc in the wild type (one biological replicate), as described by Lambing et al. (2020). In vitro cross-linking and nuclei isolation were performed in nuclei isolation cross-linking buffer (60 mM Hepes, pH 8.0, 1 M Suc, 5 mM KCl, 5 mM $MgCl_2$, 5 mM EDTA, 0.6% [v/v] Triton X-100, 0.4 mM PMSF, 1 mM pepstatin, 1× protein cocktail inhibitor, and 1% [w/v] formaldehyde) at room temperature for 25 min. Gly was added to a final concentration of 125 mM, and the nuclei solution was incubated at room temperature for an additional 25 min. The nuclei were purified from cellular debris by filtering the nuclei solution twice through one layer of Miracloth and centrifugation at 12,000*g* for 10 min at 4°C. The pellet was resuspended in EB2 buffer (0.25 M Suc, 10 mM Tris-HCl, pH 8.0, 10 mM $MgCl_2$, 1% [v/v] Triton X-100, 1 mM EDTA, 5 mM β-mercaptoethanol, 0.1 mM PMSF, 1 mM pepstatin, and 1× protein cocktail inhibitor) followed by a centrifugation at 12,000*g* for 10 min at 4°C. The supernatant was discarded, and the pellet was resuspended in nuclei lysis buffer (50 mM Tris-HCl, pH 8.0, 10 mM EDTA, 1% [v/v] SDS, 0.1 mM PMSF, 1 mM pepstatin, and 1× protein cocktail inhibitor). DNA was sonicated using a Bioruptor for 15 min (high intensity 320 W, 30 s ON – 30 s OFF). The nucleus lysis solution was then diluted (3 volumes:2 volumes) with ChIP dilution buffer (1.1% [v/v] Triton X-100, 1.1 mM EDTA, 20 mM Tris-HCl, pH 8.0, 167 mM NaCl, 1 mM pepstatin, and 1× protein cocktail inhibitor), and a second cycle of DNA sonication was performed (25 min at high intensity 320W with 30 s ON – 1 min OFF). The solution was then centrifuged at 5000*g* for 10 min at 4°C. Five percent of the supernatant was kept as a DNA input sample. The remaining supernatant was incubated with 7 μg of α-Myc (ab9132, Abcam) or 7 μg of α-HA (ab9110, Abcam) antibodies that had been prebound to 50 μL of Dynabead Protein G (10004D, Invitrogen) per gram of floral buds and was then incubated for 16 h at 4°C. The immunoprecipitate was washed two times for 5 min with low salt buffer (150 mM NaCl, 0.1% [v/v] SDS, 1% [v/v] Triton X-100, 2 mM EDTA, and 20 mM Tris-HCl, pH 8.0) and 2 times for 5 min with high salt buffer (500 mM NaCl, 0.1% [v/v] SDS, 1% [v/v] Triton X-100, 2 mM EDTA, and 20 mM Tris-HCl, pH 8.0). The proteins bound to the antibody/beads were treated with elution buffer (1% SDS and 0.1 M $NaHCO_3$) at 65°C for 10 min. DNA–protein complexes were reverse cross-linked by adding NaCl to a final concentration of 240 mM, and the solution was incubated at 65°C overnight. ChIP-DNA was purified with phenol/chloroform, and 10 ng of ChIP-purified DNA was used to generate libraries using the TruSeq DNA Sample Preparation Kit v2 (Illumina), as described by Choi et al. (2018).

ChIP-qPCR Analysis

Enrichment of DNA following α-HA ChIP was estimated by qPCR using a QuantiNova SYBR Green PCR kit (208054, Qiagen) and a CFX96 qPCR instrument (Bio-Rad). Briefly, 0.25 ng of DNA was used with 0.7 μM of primers for qPCR amplifications. The PCR program used was 40 cycles of 95°C for 2 min, 95°C for 5 s, and 60°C for 10 s. To calculate α-HA ChIP enrichment of DNA, amplifications were compared with input DNA, between *REC8-HA rec8* transgenic plants and nontransgenic Col plants.

RNA-Seq

Unopened flower buds were collected from pools of Col or *kyp suvh5 suvh6* plants to provide two biological replicates for each genotype. For each replicate, 100 mg of unopened flower buds was ground in liquid nitrogen and RNA was extracted using TRIzol reagent. Six micrograms of total RNA per sample was treated with DNase I using TURBO DNase reagents (AM2238, Thermo Fisher Scientific). Four micrograms of total DNase I–treated total RNA was then treated with Ribo-Zero rRNA Removal Kit (MRZPL116, Epicentre) to deplete rRNA from the RNA sample. Fifty nanograms of rRNA-depleted DNase I–treated RNA was used to prepare RNA-seq libraries using the ScriptSeq v2 RNA-seq Library Preparation Kit (SSV21124, Epicentre), as described by Choi et al. (2018).

ChIP-Seq Data Analysis

Deduplicated paired-end (2 × 76 bp) ChIP-seq reads were aligned to the The Arabidopsis Information Resource 10 (TAIR10) reference genome using Bowtie2 version 2.2.9 (Langmead and Salzberg, 2012), with the following settings:–very sensitive–no-discordant–no-mixed -p 4 -k 10. Up to 10 valid alignments were reported for each read. Aligned reads with more than two mismatches were discarded using the Sequence Alignment/Map (SAM) optional field XM:i. Uniquely aligning reads were extracted by removing alignments with the SAM optional field XS:i and with Bowtie2-assigned MAPping Quality (MAPQ) scores lower than 42. Alignments consisting of reads that mapped to multiple loci were filtered such that only those with MAPQ scores higher than or equal to 10 remained, from which the alignment with the highest MAPQ score was retained. Where MAPQ scores for multiple valid alignments were equal, one alignment was randomly selected. Alignments consisting of only one read in a pair were

discarded. The genome-wide average depth of coverage obtained for each library is provided in Supplemental Table 2.

Unique and multiple alignments in Binary Alignment/Map format were combined, and coverage was calculated for each coordinate in the genome using Rsamtools version 1.26.1. Coverage was normalized by the sum of coverage for each library. The $\log_2$ ratio of ChIP:input coverage was calculated to control for background and variation in mappability across genomic loci. These values were used to generate chromosome-scale coverage profiles and fine-scale coverage profiles around genome features within specific annotation categories, including REC8-HA peaks (defined as described below), well-positioned nucleosomes (Choi et al. 2018), SPO11-1-oligo hotspots (Choi et al. 2018), TAIR10 representative gene TSSs and TTSs, TEs (Buisine et al., 2008), and a set of 3320 crossover intervals mapped using genotyping by sequencing of Col × Landsberg *erecta* F_2 plants (Choi et al., 2018; Serra et al., 2018). A coverage profile was generated for each feature using the normalizeToMatrix function from the Bioconductor package EnrichedHeatmap version 1.11.1 (Gu et al., 2018). Because of varying feature lengths, each feature was divided into proportionally scaled windows between start and end coordinates, and 2-kb flanking regions were divided into 20-bp windows or 5-kb regions flanking crossovers were divided into 50-bp windows. For each window along each feature and its flanking regions, an average value was calculated using the w0 method for ChIP-seq data or the absolute method for bisulfite-sequencing data. The default profile-smoothing method implemented in the normalizeToMatrix function was applied. The resulting matrix of windowed coverage or DNA methylation proportion values was used to generate a mean profile (averaged over all features), or a heatmap in which each row represents a single feature. Mean profiles and heatmaps were plotted such that the distance between feature start and end coordinates along the *x* axis represents the mean feature length. Previously published paired-end H3K4me3 ChIP-seq and MNase-seq reads in the wild type (Choi et al., 2018) and single-end SPO11-1-oligo reads in the wild type and *kyp suvh5 suvh6* (Choi et al., 2018; Underwood et al., 2018) were aligned to the TAIR10 reference genome and processed for downstream analysis, as described previously by Choi et al. (2018).

REC8, H3K4me3, H3K9me2, and SPO11-1-oligo peaks were identified using the ranger tool within the PeakRanger suite (Feng et al., 2011) with the–pad option specified, providing ChIP input or genomic DNA (gDNA) reads as a control for background in each case. H3K4me3 and H3K9me2 peaks were defined by applying P-value and FDR thresholds of ≤0.05, with read extension lengths (–ext_length option) of 125 and 150 nucleotides specified, respectively, based on mean estimated fragment lengths derived from Binary Alignment/Map files. REC8 ChIP-seq peaks were detected using more stringent significance thresholds ($P \leq 0.001$ and FDR ≤ 0.01) and with a read extension length of 200 nucleotides specified. SPO11-1-oligo hotspots were identified as described previously by Choi et al. (2018). Any overlapping peaks were merged.

REC8-HA peaks and SPO11-1-oligo hotspots were evaluated for overlap with genomic features within other annotation categories by performing permutation tests using the Bioconductor package regioneR version 1.6.2 (Gel et al., 2016). Overlaps were defined as the number of REC8-HA peaks or SPO11-1-oligo hotspots that overlap one or more features within a given annotation category. For each test, 10,000 sets of randomly positioned loci with the same width distribution as the REC8-HA peaks or SPO11-1-oligo hotspots were defined. For each set, the number of random loci overlapping features within a given annotation category was compared with the observed number of overlapping REC8-HA peaks or SPO11-1-oligo hotspots. This provided the basis for calculating an empirical P-value ($\geq 1 \times 10^{-4}$, with the minimum obtainable P-value determined by the number of permutations) denoting the significance of the observed overlap.

Well-positioned nucleosomes were identified in mapped MNase-seq data (Choi et al., 2018), using the R package nucleR (Flores and Orozco, 2011). Well-positioned nucleosomes are defined narrow peaks in nucleosomal signal corresponding to the size of a single nucleosome core (~147 bp) and characterized by troughs in signal in flanking regions. As nucleR identifies nucleosome positions from paired-end 100-bp MNase-seq reads, these were trimmed to the central 40 bp to improve detection. Coverage at each position in the genome was calculated and normalized by library size. Paired-end reads from a Col gDNA library were processed in the same way to provide a control. These data were used to calculate $\log_2$(MNase-seq/gDNA) coverage ratios at each genomic coordinate. To remove noise from the $\log_2$(MNase-seq/gDNA) profile, the fast Fourier transform was applied using the filterFFT function within nucleR, retaining 2% of the components of the original profile (pcKeepComp = 0.02). Peaks in the signal were identified using the peakDetection function, specifying a peak width of 140 bp centered on the local maximum. Peaks with nucleR-assigned height scores greater than 0.99 were retained. Any overlapping peaks were merged. Additionally, DNA methylation proportions derived from published bisulfite sequencing reads in the wild type and *kyp suvh5 suvh6* were used to profile DNA methylation levels at chromosome and fine scales (Stroud et al., 2013).

RNA-Seq Data Analysis

For analysis of chromosome-scale and fine-scale expression profiles, paired-end (2 × 76 bp) RNA-seq reads were aligned to the TAIR10 reference genome using STAR version 2.5.3a (Dobin et al., 2013), with the following settings:–runThreadN 24–outFilterMultimapNmax 10–outFilterMismatchNmax 2–outMultimapperOrder Random–outSAMattributes All–twopassMode Basic–twopass1readsN -1. Read pairs with up to 10 valid alignments and up to two mismatches were reported as mapped. Uniquely aligned reads were extracted by selecting alignments with STAR-assigned MAPQ scores of 255. Alignments consisting of reads that mapped to multiple loci were extracted using the SAM field NH:i. Multiple alignments with MAPQ scores lower than 3 were discarded. As the maximum STAR-assigned MAPQ score for multiple alignments is 3, a primary multiple alignment was randomly selected. Alignments consisting of only one read in a pair were discarded. Unique and multiple alignments were combined, and coverage was calculated for each coordinate in the genome using Rsamtools 1.26.1. Coverage was normalized by the total coverage for each library. Analysis of differential expression between the wild type and *kyp suvh5 suvh6* mutant samples was performed using the Bioconductor package DESeq2 version 1.16.1 (Love et al., 2014), as described by Lawrence et al. (2019). TEs that were upregulated in *kyp suvh5 suvh6* relative to the wild type were evaluated for over-representation of elements within each TE superfamily using the hypergeometric distribution.

Accession Numbers

The gene accession numbers for *REC8*, *KYP*, *SUVH5*, and *SUVH6* are AT5G05490, AT5G13960, AT2G35160, and AT2G22740, respectively. ChIP-seq and RNA-seq data have been deposited in the ArrayExpress database at EMBL-EBI (www.ebi.ac.uk/arrayexpress) under accession numbers E-MTAB-7370 (ChIP-seq) and E-MTAB-7371 (RNA-seq), respectively.

Supplemental Data

Supplemental Figure 1. Detection of REC8-Myc fusion proteins via immunoblotting and immunostaining during meiosis.

Supplemental Figure 2. Overlap of REC8-HA peaks with other genome features.

Supplemental Table 1. Chiasma counts from wild-type (Col) and *REC8-HA rec8* male meiocytes at metaphase I.

Supplemental Table 2. Aligned reads from chromatin immunoprecipitation sequencing and RNA sequencing libraries.

Supplemental Table 3. Correlations between REC8-HA and REC8-Myc ChIP libraries at varying physical scales.

Supplemental Table 4. ChIP-qPCR analysis of peak enrichment in *REC8-HA rec8* and wild-type (Col) flowers.

Supplemental Table 5. Overlap of REC8-HA peaks with other genome features in chromosome arms.

Supplemental Table 6. Overlap of REC8-HA peaks with other genome features in the pericentromeres.

Supplemental Table 7. Overrepresentation analysis of TE superfamilies that are transcriptionally upregulated in *kyp suvh5 suvh6*.

Supplemental Table 8. ASY1 axis length measurements in wild type (Col) and *rec8*.

Supplemental Table 9. Inter-axis width measurements between synapsed ZYP1 structures in the wild type (Col) and *rec8.*

Supplemental Table 10. Recombination foci counts of γH2A.X, RAD51 and RPA1a in the wild type (Col) and *rec8* mid-prophase I nuclei.

Supplemental Table 11. DMC1 and MSH4 recombination foci counted in the wild type (Col) and *rec8* during mid-prophase I.

Supplemental Table 12. Correlations between axis length and recombination foci in the wild type (Col) and *rec8.*

Supplemental Table 13. MLH1 foci counts in wild-type (Col) and *rec8* nuclei at late prophase I.

Supplemental Table 14. Oligonucleotide sequences.

ACKNOWLEDGMENTS

We thank Mathilde Grelon for the MLH1 antibody and the Gurdon Institute for access to microscopes. Research was supported by the European Research Council (SynthHotSpot) and Biotechnology and Biological Sciences Research Council (grants BB/L006847/1, BB/N007557/1, and BB/N002628/1) and by the European Molecular Biology Organization (long-term postdoctoral fellowship ALTF 807-2009).

AUTHOR CONTRIBUTIONS

C.L., A.J.T., K.C., P.C.K., K.O., J.D.H., F.C.H.F., and I.R.H. designed the research; C.L., S.D.T., P.C.K., and J.D.H. performed research; C.L., A.J.T., X.Z., K.O., J.D.H., F.C.H.F., and I.R.H. analyzed data; C.L., A.J.T., K.O., J.D.H., F.C.H.F., and I.R.H. wrote the article.

Received November 7, 2019; revised January 3, 2020; accepted February 3, 2020; published February 5, 2020.

REFERENCES

Acquaviva, L., Székvölgyi, L., Dichtl, B., Dichtl, B.S., de La Roche Saint André, C., Nicolas, A., and Géli, V. (2013). The COMPASS subunit Spp1 links histone methylation to initiation of meiotic recombination. Science **339:** 215–218.

Armstrong, S. (2013). A time course for the analysis of meiotic progression in *Arabidopsis thaliana*. Methods Mol. Biol. **990:** 119–123.

Armstrong, S.J., Caryl, A.P., Jones, G.H., and Franklin, F.C.H. (2002). Asy1, a protein required for meiotic chromosome synapsis, localizes to axis-associated chromatin in Arabidopsis and Brassica. J. Cell Sci. **115:** 3645–3655.

Armstrong, S.J., Franklin, F.C., and Jones, G.H. (2001). Nucleolus-associated telomere clustering and pairing precede meiotic chromosome synapsis in *Arabidopsis thaliana*. J. Cell Sci. **114:** 4207–4217.

Barton, N.H., and Charlesworth, B. (2009). Why sex and recombination? Cold Spring Harb. Symp. Quant. Biol. **74:** 187–195.

Baudat, F., Imai, Y., and de Massy, B. (2013). Meiotic recombination in mammals: Localization and regulation. Nat. Rev. Genet. **14:** 794–806.

Bernard, P., Maure, J.F., Partridge, J.F., Genier, S., Javerzat, J.P., and Allshire, R.C. (2001). Requirement of heterochromatin for cohesion at centromeres. Science **294:** 2539–2542.

Bhatt, A.M., Lister, C., Page, T., Fransz, P., Findlay, K., Jones, G.H., Dickinson, H.G., and Dean, C. (1999). The DIF1 gene of Arabidopsis is required for meiotic chromosome segregation and belongs to the REC8/RAD21 cohesin gene family. Plant J. **19:** 463–472.

Blat, Y., Protacio, R.U., Hunter, N., and Kleckner, N. (2002). Physical and functional interactions among basic chromosome organizational features govern early steps of meiotic chiasma formation. Cell **111:** 791–802.

Bolaños-Villegas, P., De, K., Pradillo, M., Liu, D., and Makaroff, C.A. (2017). In favor of establishment: Regulation of chromatid cohesion in plants. Front. Plant Sci. **8:** 846.

Buisine, N., Quesneville, H., and Colot, V. (2008). Improved detection and annotation of transposable elements in sequenced genomes using multiple reference sequence sets. Genomics **91:** 467–475.

Busslinger, G.A., Stocsits, R.R., van der Lelij, P., Axelsson, E., Tedeschi, A., Galjart, N., and Peters, J.-M. (2017). Cohesin is positioned in mammalian genomes by transcription, CTCF and Wapl. Nature **544:** 503–507.

Cai, X., Dong, F., Edelmann, R.E., and Makaroff, C.A. (2003). The Arabidopsis SYN1 cohesin protein is required for sister chromatid arm cohesion and homologous chromosome pairing. J. Cell Sci. **116:** 2999–3007.

Chambon, A., West, A., Vezon, D., Horlow, C., De Muyt, A., Chelysheva, L., Ronceret, A., Darbyshire, A., Osman, K., Heckmann, S., Franklin, F.C.H., and Grelon, M. (2018). Identification of ASYNAPTIC4, a component of the meiotic chromosome axis. Plant Physiol. **178:** 233–246.

Chelysheva, L., et al. (2005). AtREC8 and AtSCC3 are essential to the monopolar orientation of the kinetochores during meiosis. J. Cell Sci. **118:** 4621–4632.

Chelysheva, L., Grandont, L., Vrielynck, N., le Guin, S., Mercier, R., and Grelon, M. (2010). An easy protocol for studying chromatin and recombination protein dynamics during *Arabidopsis thaliana* meiosis: Immunodetection of cohesins, histones and MLH1. Cytogenet. Genome Res. **129:** 143–153.

Choi, K., and Henderson, I.R. (2015). Meiotic recombination hotspots - A comparative view. Plant J. **83:** 52–61.

Choi, K., et al. (2016). Recombination rate heterogeneity within Arabidopsis disease resistance genes. PLoS Genet. **12:** e1006179.

Choi, K., et al. (2018). Nucleosomes and DNA methylation shape meiotic DSB frequency in *Arabidopsis thaliana* transposons and gene regulatory regions. Genome Res. **28:** 532–546.

Choi, K., Zhao, X., Kelly, K.A., Venn, O., Higgins, J.D., Yelina, N.E., Hardcastle, T.J., Ziolkowski, P.A., Copenhaver, G.P., Franklin, F.C.H., McVean, G., and Henderson, I.R. (2013). Arabidopsis meiotic crossover hot spots overlap with H2A.Z nucleosomes at gene promoters. Nat. Genet. **45:** 1327–1336.

da Costa-Nunes, J.A., Capitão, C., Kozak, J., Costa-Nunes, P., Ducasa, G.M., Pontes, O., and Angelis, K.J. (2014). The AtRAD21.1 and AtRAD21.3 Arabidopsis cohesins play a synergistic role in somatic DNA double strand break damage repair. BMC Plant Biol. **14:** 353.

d'Erfurth, I., Jolivet, S., Froger, N., Catrice, O., Novatchkova, M., and Mercier, R. (2009). Turning meiosis into mitosis. PLoS Biol. **7:** e1000124.

Dobin, A., Davis, C.A., Schlesinger, F., Drenkow, J., Zaleski, C., Jha, S., Batut, P., Chaisson, M., and Gingeras, T.R. (2013). STAR: Ultrafast universal RNA-seq aligner. Bioinformatics **29:** 15–21.

Ellermeier, C., Higuchi, E.C., Phadnis, N., Holm, L., Geelhood, J.L., Thon, G., and Smith, G.R. (2010). RNAi and heterochromatin repress centromeric meiotic recombination. Proc. Natl. Acad. Sci. USA **107:** 8701–8705.

Feng, X., Grossman, R., and Stein, L. (2011). PeakRanger: A cloud-enabled peak caller for ChIP-seq data. BMC Bioinformatics **12:** 139.

Ferdous, M., Higgins, J.D., Osman, K., Lambing, C., Roitinger, E., Mechtler, K., Armstrong, S.J., Perry, R., Pradillo, M., Cuñado, N., and Franklin, F.C.H. (2012). Inter-homolog crossing-over and synapsis in Arabidopsis meiosis are dependent on the chromosome axis protein AtASY3. PLoS Genet. **8:** e1002507.

Flores, O., and Orozco, M. (2011). nucleR: A package for non-parametric nucleosome positioning. Bioinformatics **27:** 2149–2150.

Folco, H.D., Chalamcharla, V.R., Sugiyama, T., Thillainadesan, G., Zofall, M., Balachandran, V., Dhakshnamoorthy, J., Mizuguchi, T., and Grewal, S.I.S. (2017). Untimely expression of gametogenic genes in vegetative cells causes uniparental disomy. Nature **543:** 126–130.

Fowler, K.R., Sasaki, M., Milman, N., Keeney, S., and Smith, G.R. (2014). Evolutionarily diverse determinants of meiotic DNA break and recombination landscapes across the genome. Genome Res. **24:** 1650–1664.

Gel, B., Díez-Villanueva, A., Serra, E., Buschbeck, M., Peinado, M.A., and Malinverni, R. (2016). regioneR: An R/Bioconductor package for the association analysis of genomic regions based on permutation tests. Bioinformatics **32:** 289–291.

Glynn, E.F., Megee, P.C., Yu, H.-G., Mistrot, C., Unal, E., Koshland, D.E., DeRisi, J.L., and Gerton, J.L. (2004). Genome-wide mapping of the cohesin complex in the yeast *Saccharomyces cerevisiae*. PLoS Biol. **2:** E259.

Gu, Z., Eils, R., Schlesner, M., and Ishaque, N. (2018). EnrichedHeatmap: An R/Bioconductor package for comprehensive visualization of genomic signal associations. BMC Genomics **19:** 234.

Guenatri, M., Bailly, D., Maison, C., and Almouzni, G. (2004). Mouse centric and pericentric satellite repeats form distinct functional heterochromatin. J. Cell Biol. **166:** 493–505.

He, Y., et al. (2017). Genomic features shaping the landscape of meiotic double-strand-break hotspots in maize. Proc. Natl. Acad. Sci. USA **114:** 12231–12236.

Higgins, J.D., Armstrong, S.J., Franklin, F.C.H., and Jones, G.H. (2004). The Arabidopsis MutS homolog AtMSH4 functions at an early step in recombination: Evidence for two classes of recombination in Arabidopsis. Genes Dev. **18:** 2557–2570.

Higgins, J.D., Sanchez-Moran, E., Armstrong, S.J., Jones, G.H., and Franklin, F.C.H. (2005). The Arabidopsis synaptonemal complex protein ZYP1 is required for chromosome synapsis and normal fidelity of crossing over. Genes Dev. **19:** 2488–2500.

Hinshaw, S.M., Makrantoni, V., Harrison, S.C., and Marston, A.L. (2017). The kinetochore receptor for the cohesin loading complex. Cell **171:** 72–84.e13.

Hong, S., Sung, Y., Yu, M., Lee, M., Kleckner, N., and Kim, K.P.P. (2013). The logic and mechanism of homologous recombination partner choice. Mol. Cell **51:** 440–453.

Ito, M., Kugou, K., Fawcett, J.A., Mura, S., Ikeda, S., Innan, H., and Ohta, K. (2014). Meiotic recombination cold spots in chromosomal cohesion sites. Genes Cells **19:** 359–373.

Jacob, Y., Feng, S., LeBlanc, C.A., Bernatavichute, Y.V., Stroud, H., Cokus, S., Johnson, L.M., Pellegrini, M., Jacobsen, S.E., and Michaels, S.D. (2009). ATXR5 and ATXR6 are H3K27 monomethyltransferases required for chromatin structure and gene silencing. Nat. Struct. Mol. Biol. **16:** 763–768.

Kauppi, L., Jeffreys, A.J., and Keeney, S. (2004). Where the crossovers are: Recombination distributions in mammals. Nat. Rev. Genet. **5:** 413–424.

Kianian, P.M.A., et al. (2018). High-resolution crossover mapping reveals similarities and differences of male and female recombination in maize. Nat. Commun. **9:** 2370.

Kim, K.P., Weiner, B.M., Zhang, L., Jordan, A., Dekker, J., and Kleckner, N. (2010). Sister cohesion and structural axis components mediate homolog bias of meiotic recombination. Cell **143:** 924–937.

Kitajima, T.S., Miyazaki, Y., Yamamoto, M., and Watanabe, Y. (2003). Rec8 cleavage by separase is required for meiotic nuclear divisions in fission yeast. EMBO J. **22:** 5643–5653.

Klein, F., Mahr, P., Galova, M., Buonomo, S.B., Michaelis, C., Nairz, K., and Nasmyth, K. (1999). A central role for cohesins in sister chromatid cohesion, formation of axial elements, and recombination during yeast meiosis. Cell **98:** 91–103.

Koch, B., Kueng, S., Ruckenbauer, C., Wendt, K.S., and Peters, J.-M. (2008). The Suv39h-HP1 histone methylation pathway is dispensable for enrichment and protection of cohesin at centromeres in mammalian cells. Chromosoma **117:** 199–210.

Kugou, K., Fukuda, T., Yamada, S., Ito, M., Sasanuma, H., Mori, S., Katou, Y., Itoh, T., Matsumoto, K., Shibata, T., Shirahige, K., and Ohta, K. (2009). Rec8 guides canonical Spo11 distribution along yeast meiotic chromosomes. Mol. Biol. Cell **20:** 3064–3076.

Laloraya, S., Guacci, V., and Koshland, D. (2000). Chromosomal addresses of the cohesin component Mcd1p. J. Cell Biol. **151:** 1047–1056.

Lam, I., and Keeney, S. (2014). Mechanism and regulation of meiotic recombination initiation. Cold Spring Harb. Perspect. Biol. **7:** a016634.

Lambing, C., Choi, K., Blackwell, A.R., and Henderson, I.R. (2020). Chromatin immunoprecipitation of meiotically expressed proteins from *Arabidopsis thaliana* flowers. Methods Mol. Biol. **2061:** 219–236.

Lambing, C., Osman, K., Nuntasoontorn, K., West, A., Higgins, J.D., Copenhaver, G.P., Yang, J., Armstrong, S.J., Mechtler, K., Roitinger, E., and Franklin, F.C.H. (2015). Arabidopsis PCH2 mediates meiotic chromosome remodeling and maturation of crossovers. PLoS Genet. **11:** e1005372.

Lange, J., Yamada, S., Tischfield, S.E., Pan, J., Kim, S., Zhu, X., Socci, N.D., Jasin, M., and Keeney, S. (2016). The landscape of mouse meiotic double-strand break formation, processing, and repair. Cell **167:** 695–708.

Langmead, B., and Salzberg, S.L. (2012). Fast gapped-read alignment with Bowtie 2. Nat. Methods **9:** 357–359.

Law, J.A., and Jacobsen, S.E. (2010). Establishing, maintaining and modifying DNA methylation patterns in plants and animals. Nat. Rev. Genet. **11:** 204–220.

Lawrence, E.J., Gao, H., Tock, A.J., Lambing, C., Blackwell, A.R., Feng, X., and Henderson, I.R. (2019). Natural variation in TBP-ASSOCIATED FACTOR 4b controls meiotic crossover and germline transcription in Arabidopsis. Curr. Biol. **29:** 2676–2686.e3.

Lee, T.F., Gurazada, S.G.R., Zhai, J., Li, S., Simon, S.A., Matzke, M.A., Chen, X., and Meyers, B.C. (2012). RNA polymerase

V-dependent small RNAs in Arabidopsis originate from small, intergenic loci including most SINE repeats. Epigenetics **7:** 781–795.

Lengronne, A., Katou, Y., Mori, S., Yokobayashi, S., Kelly, G.P., Itoh, T., Watanabe, Y., Shirahige, K., and Uhlmann, F. (2004). Cohesin relocation from sites of chromosomal loading to places of convergent transcription. Nature **430:** 573–578.

Liu, S., Yeh, C.-T., Ji, T., Ying, K., Wu, H., Tang, H.M., Fu, Y., Nettleton, D., and Schnable, P.S. (2009). Mu transposon insertion sites and meiotic recombination events co-localize with epigenetic marks for open chromatin across the maize genome. PLoS Genet. **5:** e1000733.

Love, M.I., Huber, W., and Anders, S. (2014). Moderated estimation of fold change and dispersion for RNA-seq data with DESeq2. Genome Biol. **15:** 550.

Maheshwari, S., Ishii, T., Brown, C.T., Houben, A., and Comai, L. (2017). Centromere location in *Arabidopsis* is unaltered by extreme divergence in CENH3 protein sequence. Genome Res. **27:** 471–478.

Mancera, E., Bourgon, R., Brozzi, A., Huber, W., and Steinmetz, L.M. (2008). High-resolution mapping of meiotic crossovers and non-crossovers in yeast. Nature **454:** 479–485.

de Massy, B. (2013). Initiation of meiotic recombination: How and where? Conservation and specificities among eukaryotes. Annu. Rev. Genet. **47:** 563–599.

Mercier, R., Mézard, C., Jenczewski, E., Macaisne, N., and Grelon, M. (2015). The molecular biology of meiosis in plants. Annu. Rev. Plant Biol. **66:** 297–327.

Mizuguchi, T., Fudenberg, G., Mehta, S., Belton, J.-M., Taneja, N., Folco, H.D., FitzGerald, P., Dekker, J., Mirny, L., Barrowman, J., and Grewal, S.I.S. (2014). Cohesin-dependent globules and heterochromatin shape 3D genome architecture in S. pombe. Nature **516:** 432–435.

Neale, M.J., Pan, J., and Keeney, S. (2005). Endonucleolytic processing of covalent protein-linked DNA double-strand breaks. Nature **436:** 1053–1057.

Nonaka, N., Kitajima, T., Yokobayashi, S., Xiao, G., Yamamoto, M., Grewal, S.I.S., and Watanabe, Y. (2002). Recruitment of cohesin to heterochromatic regions by Swi6/HP1 in fission yeast. Nat. Cell Biol. **4:** 89–93.

Osman, K., Sanchez-Moran, E., Mann, S.C., Jones, G.H., and Franklin, F.C.H. (2009). Replication protein A (AtRPA1a) is required for class I crossover formation but is dispensable for meiotic DNA break repair. EMBO J. **28:** 394–404.

Osman, K., Yang, J., Roitinger, E., Lambing, C., Heckmann, S., Howell, E., Cuacos, M., Imre, R., Dürnberger, G., Mechtler, K., Armstrong, S., and Franklin, F.C.H. (2018). Affinity proteomics reveals extensive phosphorylation of the Brassica chromosome axis protein ASY1 and a network of associated proteins at prophase I of meiosis. Plant J. **93:** 17–33.

Page, S.L., and Hawley, R.S. (2003). Chromosome choreography: The meiotic ballet. Science **301:** 785–789.

Pan, J., Sasaki, M., Kniewel, R., Murakami, H., Blitzblau, H.G., Tischfield, S.E., Zhu, X., Neale, M.J., Jasin, M., Socci, N.D., Hochwagen, A., and Keeney, S. (2011). A hierarchical combination of factors shapes the genome-wide topography of yeast meiotic recombination initiation. Cell **144:** 719–731.

Ross, K.J., Fransz, P., and Jones, G.H. (1996). A light microscopic atlas of meiosis in *Arabidopsis thaliana*. Chromosome Res. **4:** 507–516.

Rowan, B.A., Heavens, D., Feuerborn, T.R., Tock, A.J., Henderson, I.R., and Weigel, D. (2019). An ultra high-density *Arabidopsis thaliana* crossover map that refines the influences of structural variation and epigenetic features. Genetics **213:** 771–787.

Sanchez-Moran, E., Santos, J.-L., Jones, G.H., and Franklin, F.C.H. (2007). ASY1 mediates AtDMC1-dependent interhomolog recombination during meiosis in Arabidopsis. Genes Dev. **21:** 2220–2233.

Schmidt, C.K., Brookes, N., and Uhlmann, F. (2009). Conserved features of cohesin binding along fission yeast chromosomes. Genome Biol. **10:** R52.

Segal, E., and Widom, J. (2009). Poly(dA:dT) tracts: Major determinants of nucleosome organization. Curr. Opin. Struct. Biol. **19:** 65–71.

Serra, H., Lambing, C., Griffin, C.H., Topp, S.D., Nageswaran, D.C., Underwood, C.J., Ziolkowski, P.A., Séguéla-Arnaud, M., Fernandes, J.B., Mercier, R., and Henderson, I.R. (2018). Massive crossover elevation via combination of *HEI10* and *recq4a recq4b* during *Arabidopsis* meiosis. Proc. Natl. Acad. Sci. USA **115:** 2437–2442.

Sommermeyer, V., Béneut, C., Chaplais, E., Serrentino, M.E., and Borde, V. (2013). Spp1, a member of the Set1 complex, promotes meiotic DSB formation in promoters by tethering histone H3K4 methylation sites to chromosome axes. Mol. Cell **49:** 43–54.

Stigler, J., Çamdere, G., Koshland, D.E., and Greene, E.C. (2016). Single-molecule imaging reveals a collapsed conformational state for DNA-bound cohesin. Cell Rep. **15:** 988–998.

Stroud, H., Do, T., Du, J., Zhong, X., Feng, S., Johnson, L., Patel, D.J., and Jacobsen, S.E. (2014). Non-CG methylation patterns shape the epigenetic landscape in Arabidopsis. Nat. Struct. Mol. Biol. **21:** 64–72.

Stroud, H., Greenberg, M.V.C., Feng, S., Bernatavichute, Y.V., and Jacobsen, S.E. (2013). Comprehensive analysis of silencing mutants reveals complex regulation of the Arabidopsis methylome. Cell **152:** 352–364.

Sun, X., Huang, L., Markowitz, T.E., Blitzblau, H.G., Chen, D., Klein, F., and Hochwagen, A. (2015). Transcription dynamically patterns the meiotic chromosome-axis interface. eLife **4.**

Topp, C.N., and Dawe, R.K. (2006). Reinterpreting pericentromeric heterochromatin. Curr. Opin. Plant Biol. **9:** 647–653.

Underwood, C.J., Choi, K., Lambing, C., Zhao, X., Serra, H., Borges, F., Simorowski, J., Ernst, E., Jacob, Y., Henderson, I.R., and Martienssen, R.A. (2018). Epigenetic activation of meiotic recombination near *Arabidopsis thaliana* centromeres via loss of H3K9me2 and non-CG DNA methylation. Genome Res. **28:** 519–531.

Villeneuve, A.M., and Hillers, K.J. (2001). Whence meiosis? Cell **106:** 647–650.

Vincenten, N., Kuhl, L.-M., Lam, I., Oke, A., Kerr, A.R., Hochwagen, A., Fung, J., Keeney, S., Vader, G., and Marston, A.L. (2015). The kinetochore prevents centromere-proximal crossover recombination during meiosis. eLife **4:** e10850.

Walker, J., Gao, H., Zhang, J., Aldridge, B., Vickers, M., Higgins, J.D., and Feng, X. (2018). Sexual-lineage-specific DNA methylation regulates meiosis in Arabidopsis. Nat. Genet. **50:** 130–137.

Watanabe, Y., and Nurse, P. (1999). Cohesin Rec8 is required for reductional chromosome segregation at meiosis. Nature **400:** 461–464.

West, A.M., Rosenberg, S.C., Ur, S.N., Lehmer, M.K., Ye, Q., Hagemann, G., Caballero, I., Usón, I., MacQueen, A.J., Herzog, F., and Corbett, K.D. (2019). A conserved filamentous assembly underlies the structure of the meiotic chromosome axis. eLife **8:** e40372.

Wijnker, E., et al. (2013). The genomic landscape of meiotic crossovers and gene conversions in *Arabidopsis thaliana*. eLife **2:** e01426.

Yelagandula, R., et al. (2014). The histone variant H2A.W defines heterochromatin and promotes chromatin condensation in Arabidopsis. Cell **158:** 98–109.

Yelina, N.E., Lambing, C., Hardcastle, T.J., Zhao, X., Santos, B., and Henderson, I.R. (2015). DNA methylation epigenetically

silences crossover hot spots and controls chromosomal domains of meiotic recombination in Arabidopsis. Genes Dev. **29:** 2183–2202.

Yoon, S.-W., Lee, M.-S., Xaver, M., Zhang, L., Hong, S.-G., Kong, Y.-J., Cho, H.-R., Kleckner, N., and Kim, K.P. (2016). Meiotic prophase roles of Rec8 in crossover recombination and chromosome structure. Nucleic Acids Res. **44:** 9296–9314.

Zhang, W., Lee, H.-R., Koo, D.-H., and Jiang, J. (2008). Epigenetic modification of centromeric chromatin: Hypomethylation of DNA sequences in the CENH3-associated chromatin in *Arabidopsis thaliana* and maize. Plant Cell **20:** 25–34.

Zhu, B., Zhang, W., Zhang, T., Liu, B., and Jiang, J. (2015). Genome-wide prediction and validation of intergenic enhancers in Arabidopsis using open chromatin signatures. Plant Cell **27:** 2415–2426.

Zickler, D., and Kleckner, N. (1999). Meiotic chromosomes: Integrating structure and function. Annu. Rev. Genet. **33:** 603–754.